Westinghouse Non-Proprietary Class 3

WCAP-15885
Revision 0

July 2002

R. E. Ginna Heatup and Cooldown Limit Curves for Normal Operation

Westinghouse

WCAP-15885, Revision 0

R.E. Ginna
Heatup and Cooldown Limit Curves for Normal Operation

T. J. Laubham

JULY 2002

Prepared by the Westinghouse Electric Company LLC
for the Rochester Gas and Electric Corporation

Approved: _____
J. A. Gresham, Manager
Engineering and Materials Technology

Westinghouse Electric Company LLC
Energy Systems
P.O. Box 355
Pittsburgh, PA 15230-0355

©2002 Westinghouse Electric Company LLC
All Rights Reserved

PREFACE

This report has been technically reviewed and verified by:

J.H. Ledger	J. H. Ledger	Sections 1, 2, 4, 5, 6 and 7
S.L. Anderson	S. L. Anderson	Section 3 Only

TABLE OF CONTENTS

LIST OF TABLES iv

LIST OF FIGURES vi

EXECUTIVE SUMMARY vii

1 INTRODUCTION 1

2 FRACTURE TOUGHNESS PROPERTIES 2

3 RADIATION ANALYSIS AND NEUTRON DOSIMETRY 9

4 CRITERIA FOR ALLOWABLE PRESSURE-TEMPERATURE RELATIONSHIPS 34

5 CALCULATION OF ADJUSTED REFERENCE TEMPERATURE 38

6 HEATUP AND COOLDOWN PRESSURE-TEMPERATURE LIMIT CURVES 43

7 REFERENCES 50

LIST OF TABLES

Table 1 Summary of the Best Estimate Cu and Ni Weight Percent and Initial RT_{NDT} Values for the R.E. Ginna Reactor Vessel Materials 3

Table 2 Inlet (Tcold) Operating Temperatures 4

Table 3 Calculated Integrated Neutron Exposure of the Surveillance Capsules @ R.E. Ginna, Turkey Point Units 3 &4, Davis-Besse 5

Table 4 Calculation of Chemistry Factors using R.E. Ginna, Turkey Point Units 3 &4 and Davis-Besse Surveillance Capsule Data 6

Table 5 Summary of the R.E. Ginna Reactor Vessel Beltline Material Chemistry Factors 8

Table 6 Summary of Calculated Maximum Pressure Vessel Exposure Clad/Base Metal Interface 14

Table 7 Summary of Calculated Maximum Exposure of the Intermediate to Nozzle Shell Circumferential Weld and the Nozzle Shell Course Clad/Base Metal Interface 15

Table 8 Calculated Surveillance Capsule Exposure 16

Table 9 Calculated Surveillance Capsule Lead Factors 16

Table 10 Measured Sensor Specific Activities and Reaction Rates (Capsule V) 20

Table 11 Measured Sensor Specific Activities and Reaction Rates (Capsule R) 21

Table 12 Measured Sensor Specific Activities and Reaction Rates (Capsule T) 22

Table 13 Measured Sensor Specific Activities and Reaction Rates (Capsule S) 23

Table 14 Summary of Sensor Reaction Rates from Capsules V, R, T, and S 24

Table 15 Comparison of Measured, Calculated, and Best Estimate Reaction Rates at the Surveillance Capsule Center 29

Table 16 Comparison of Calculated and Best Estimate Exposure Parameters at the Surveillance Capsule Center 31

Table 17 Comparison of Measured and Calculated Neutron Sensor Reaction Rates For In-Vessel Surveillance Capsules V, R, T, and S 33

Table 18 Comparison of Best Estimate and Calculated Fast Neutron Exposure Rates For In-Vessel Surveillance Capsules V, R, T, and S 33

LIST OF TABLES

Table 19 Summary of the Vessel Surface, 1/4T and 3/4T Fluence Values used for the Generation of the 52 EFPY Heatup/Cooldown Curves 39

Table 20 Summary of the Calculated Fluence Factors used for the Generation of the 52 EFPY Heatup and Cooldown Curves 39

Table 21 Calculation of the ART Values for the 1/4T Location @ 52 EFPY 40

Table 22 Calculation of the ART Values for the 3/4T Location @ 52 EFPY 41

Table 23 Summary of the Limiting ART Values Used in the Generation of the R.E. Ginna Heatup/Cooldown Curves 42

Table 24 52 EFPY Heatup Curve Data Points Using 1996 App. G & ASME Code Case N-641 (without Uncertainties for Instrumentation Errors) 47

Table 25 52 EFPY Cooldown Curve Data Points Using 1996 App. G & ASME Code Case N-641 (without Uncertainties for Instrumentation Errors) 49

LIST OF FIGURES

Figure 1 R.E. Ginna r, θ Reactor Geometry at the core Midplane 12

Figure 2 R.E. Ginna r,z Geometry 13

Figure 3 R.E. Ginna Reactor Coolant System Heatup Limitations (Heatup Rates of 60 & 100°F/hr) Applicable for the First 52 EFPY (Without Margins for Instrumentation Errors) Using 1996 App. G Methodology 45

Figure 4 R.E. Ginna Reactor Coolant System Cooldown Limitations (Cooldown Rates up to 100°F/hr) Applicable for the First 52 EFPY (Without Margins for Instrumentation Errors) Using 1996 App. G Methodology 46

EXECUTIVE SUMMARY

This report provides the methodology and results of the generation of heatup and cooldown pressure temperature (PT) limit curves for normal operation of the R.E. Ginna reactor vessel. The PT curves were generated based on the latest available reactor vessel information and updated fluences. The new R.E. Ginna heatup and cooldown pressure-temperature limit curves were generated using the "axial flaw" methodology of 1995 ASME Code, Section XI through the 1996 Addenda. In addition, the PT curves were developed using ASME Code Case N-641, which allows the use of the K_{Ic} methodology (ASME Code Case N-640) and the relaxed "circ. flaw" methodology (ASME Code Case N-588).

The material with the highest adjusted reference temperature (ART) was the intermediate to lower shell girth weld seam. However, as it turns out, the intermediate shell forging is limiting for the lower temperature portion of the PT curves despite having a lower set of ART values. This is due to the fact that the higher ART values come from a circumferential weld and ASME Code Case N-641 (or N-588) allows for less restrictive methodology when a circumferential weld has the higher ART values. Thus, composite heatup and cooldown PT curves were developed from two different sets of PT curves: 1) PT curves using the highest ART values from the Intermediate to lower shell girth weld seam with the "circ flaw" methodology (Code Case N-641 or N-588), and 2) PT curves using the highest "axial flaw" ART values (which are lower than the "Circ flaw ART values) with the "axial flaw" methodology (1996 ASME Code).

1 INTRODUCTION

Heatup and cooldown limit curves are calculated using the adjusted RT_{NDT} (reference nil-ductility temperature) corresponding to the limiting beltline region material of the reactor vessel. The adjusted RT_{NDT} of the limiting material in the core region of the reactor vessel is determined by using the unirradiated reactor vessel material fracture toughness properties, estimating the radiation-induced ΔRT_{NDT}, and adding a margin. The unirradiated RT_{NDT} is designated as the higher of either the drop weight nil-ductility transition temperature (NDTT) or the temperature at which the material exhibits at least 50 ft-lb of impact energy and 35-mil lateral expansion (normal to the major working direction) minus 60°F.

RT_{NDT} increases as the material is exposed to fast-neutron radiation. Therefore, to find the most limiting RT_{NDT} at any time period in the reactor's life, ΔRT_{NDT} due to the radiation exposure associated with that time period must be added to the unirradiated RT_{NDT} (IRT_{NDT}). The extent of the shift in RT_{NDT} is enhanced by certain chemical elements (such as copper and nickel) present in reactor vessel steels. The Nuclear Regulatory Commission (NRC) has published a method for predicting radiation embrittlement in Regulatory Guide 1.99, Revision 2, "Radiation Embrittlement of Reactor Vessel Materials."[1] Regulatory Guide 1.99, Revision 2, is used for the calculation of Adjusted Reference Temperature (ART) values (IRT_{NDT} + ΔRT_{NDT} + margins for uncertainties) at the 1/4T and 3/4T locations, where T is the thickness of the vessel at the beltline region measured from the clad/base metal interface.

The heatup and cooldown curves documented in this report were generated using the most limiting ART values and the NRC approved methodology documented in WCAP-14040-NP-A, Revision 2[2], "Methodology Used to Develop Cold Overpressure Mitigating System Setpoints and RCS Heatup and Cooldown Limit Curves" with exception of the following: 1) **The fluence values used in this report are calculated fluence values (i.e. comply with Reg. Guide 1.190), not the best estimate fluence values.** 2) The K_{Ic} critical stress intensities are used in place of the K_{Ia} critical stress intensities. This methodology is taken from approved ASME Code Case N-641[3] (which covers Code Cases N-640 and N-588). 3) The 1996 Version of Appendix G to Section XI[4] will be used rather than the 1989 version.

The purpose of this report is to present the calculations and the development of the R.E. Ginna heatup and cooldown curves for 52 EFPY. This report documents the neutron fluence evaluation, the calculated ART values and the development of the PT limit curves for normal operation. The PT curves herein were generated without instrumentation errors. The PT curves include a hydrostatic leak test limit curve from 2485 psig to 1500 psig, along with the pressure-temperature limits for the vessel flange region per the requirements of 10 CFR Part 50, Appendix G[5].

2 FRACTURE TOUGHNESS PROPERTIES

The fracture-toughness properties of the ferritic materials in the reactor coolant pressure boundary are determined in accordance with the NRC Standard Review Plan [6]. The beltline material properties of the R.E. Ginna reactor vessel are presented in Table 1.

Best estimate copper (Cu) and nickel (Ni) weight percent values used to calculate chemistry factors (CF) in accordance with Regulatory Guide 1.99, Revision 2, are provided in Table 1. Additionally, surveillance capsule data is available for four capsules (Capsules V, R, T and S) already removed from the R.E. Ginna reactor vessel. This surveillance capsule data was also used to calculate CF values per Position 2.1 of Regulatory Guide 1.99, Revision 2 in Table 4. These CF values are summarized in Table 5. It should be noted that in addition to R.E. Ginna, surveillance weld data from Turkey Point Unit 3 and 4 and Davis-Besse was used in the determination of CF for the nozzle to intermediate shell girth weld of heat # 71249. Per WCAP-15092, Revision 3[7], the weld heat # 71249 was determined to be not credible. It should be noted here that the intermediate shell forging was determined not to be credible, while the lower shell forging and the intermediate to lower shell girth weld seam were determined to be credible.

The Regulatory Guide 1.99, Revision 2 methodology used to develop the heatup and cooldown curves documented in this report is the same as that documented in WCAP-14040, Revision 2.

TABLE 1
Summary of the Best Estimate Cu and Ni Weight Percent and Initial RT_{NDT} Values for the R.E. Ginna Reactor Vessel Materials

Material Description	Cu (%)[a]	Ni(%)[a]	Initial RT_{NDT}[b]
Closure Head Flange	n/a	n/a	-75°F
Vessel Flange	n/a	n/a	-52°F
Nozzle Shell Forging 123P118[a]	0.07	0.68	30°F
Intermediate Shell Forging 125S255[a]	0.07	0.69	20°F
Lower Shell Forging 125P666[a]	0.05	0.69	40°F
Nozzle to Intermediate Shell Girth Weld (Heat # 71249)[c]	0.23	0.59	10°F
Intermediate Shell to Lower Shell Girth Weld (Heat # 61782)[d]	0.25	0.56	-4.8°F
Ginna Surveillance Weld (Heat # 61782)[e]	0.23	0.53	- - -

Notes:

(a) The Cu & Ni for the forgings were taken from material, WCAP-7254[8], WCAP-14684[9] or RVID2. For the inter. & lower shell forgings, RVID2 has 0.68 Ni, however, the material cert. has 0.69 Ni. Thus, the higher Ni value will be used in the calculations. The nozzle forging copper value was not reported on the material cert, thus, per RG. 1.99 one should assume 0.35 unless justification is provided. Since the nozzle forging is made from the same material as the inter. & lower shell forgings at the same time period, it is a safe assumption to say the copper value would equal the highest Cu value from the known forgings on the vessel (i.e. 0.07).

(b) The Initial RT_{NDT} values are measured values unless otherwise noted. The values were obtained from RVID2 or WCAP-14684[9].

(c) The nozzle shell to inter. shell girth weld was fabricated from weld wire heat # 71249 Linde 80, flux Lot 8445. This is the exact heat and flux as the inter. to lower shell girth weld on the Turkey Point Units 3 & 4 Reactor Vessel. It is also identical to the Turkey Point 3 & 4 Surv. weld material. The best estimate Cu & Ni was taken from WCAP-15092 R.3[7]. This differs from RVID2 for Ginna but not for Turkey Pt. (Ref. BAW 2325).

(d) The intermediate shell to lower shell girth weld was fabricated from weld wire heat number 61782 Linde 80, flux Lot 8350. This is the same heat surveillance weld material (flux lot is 8346), but differ flux lot. The best estimate Cu & Ni was taken from WCAP-14684[9] and RVID2.

(e) The Ginna surveillance weld best estimate average Cu & Ni was determined from one unirradiated sample[8 or 10], one irradiated sample from Cap. T (Specimen W26)[10], two irradiated samples from reconstituted specimens Cap. T, and 4) Eight irradiated samples from Cap. S (W22, W23, W27, W28, W32, W35, W36 and W37)[9].

The chemistry factors were calculated using Regulatory Guide 1.99 Revision 2, Positions 1.1 and 2.1. Position 1.1 uses the Tables from the Reg. Guide along with the best estimate copper and nickel weight percents. Position 2.1 uses the surveillance capsule data from all capsules withdrawn to date. The fluence values used to determine the CFs in Table 4 are the calculated fluence values at the surveillance capsule locations. Hence, the calculated fluence values were used for all cases.

In order to account for operating temperature differences, the measured ΔRT_{NDT} values from the Turkey Point Units 3 and 4 and Davis-Besse surveillance weld data (heat #71249) were adjusted so it can be applied to the R.E. Ginna nozzle to intermediate shell girth weld, which is of the same heat. No adjustment for chemistry was necessary since the overall best estimate Cu and Ni for heat 71249 is higher than the surveillance specimen average Cu and Ni (i.e. a ratio less than 1.0)[7]. The measured ΔRT_{NDT} values from the intermediate to lower shell girth weld, which is contained in the R.E. Ginna surveillance program, were adjusted for chemistry using the ratio procedure given in Position 2.1 of Regulatory Guide 1.99, Revision 2. See Table 2 below for the Tcold operating temperatures at R.E. Ginna, Turkey Point and Davis-Besse.

TABLE 2
Inlet (Tcold) Operating Temperatures

Ginna	Turkey Point	Davis Besse
549°F (Average)*	546°F (Average)[7]	555°F (Average)[7]

* Average of the Tcold values for each Capsule removed to date for R.E. Ginna documented in the E900 Database. Current Tcold is 531°F, which started in 1996. This value will be used in future evaluations with subsequent capsule withdrawals

Contained in Table 3 are the calculated fluence values for the four capsules removed from the Ginna reactor vessel to date. Also included are the Calculated fluence values for Turkey Point Units 3 and 4 and Davis Besse. The Ginna fluence values are documented in Section 3 of this report. They were determined using ENDF/B-VI cross-sections and followed the guidance in Regulatory Guide 1.190[11]. The best available fluence information for Turkey Point Unit 3 and 4 comes from WCAP-14044[12]. The calculated fluences in WCAP-14044 were determined using ENDF/B-IV cross-sections. Thus, for conservatism the calculated fluences were increased 15% to account for going to ENDF/B-VI. [Note that WCAP-15092 Rev. 3 used the higher measured fluences from WCAP-14044] The Davis Besse material was partially irradiated at Turkey Point and Davis Besse. Per Turkey Point document PTN-ENG-SESJ-99- 0118 Revision 01 (which is a reference in WCAP-15092 Rev. 3), the cumulative measured fluence was 2.57 E19 n/cm^2. Since this too was determined using ENDF/B-IV cross-sections, then it will be increased 15% as well. This should be conservative since 15% times the calculated fluences from WCAP-14044 will not increase above the measured fluences.

TABLE 3
Calculated Integrated Neutron Exposure of the Surveillance Capsules
@ R.E. Ginna, Turkey Point Units 3 & 4, Davis-Besse

Capsule	Fluence
Ginna Capsule Fluences	
V	5.87×10^{18} n/cm^2, (E > 1.0 MeV)
R	1.02×10^{19} n/cm^2, (E > 1.0 MeV)
S	1.69×10^{19} n/cm^2, (E > 1.0 MeV)
T	3.64×10^{19} n/cm^2, (E > 1.0 MeV)
Turkey Point Unit 3 Capsule Fluences[a]	
T	6.99×10^{18} n/cm^2, (E > 1.0 MeV)
V	1.484×10^{19} n/cm^2, (E > 1.0 MeV)
Turkey Point Unit 4 Capsule Fluences[a]	
T	6.73×10^{18} n/cm^2, (E > 1.0 MeV)
Davis Besse- Turkey Point Unit 3 Combined Capsule Fluences[b]	
V	2.956×10^{19} n/cm^2, (E > 1.0 MeV)

NOTES:

(a) Per WCAP-14044 and increased 15% to account for ENDF/B-VI Cross-sections.

(b) Per Turkey Point document PTN-ENG-SESJ-99- 0118 Revision 01[7], the fluence is combined between Turkey Point and Davis Besse equivalent to 2.57 E19. This value was also increased 15% to account for ENDF/B-VI cross-sections.

TABLE 4

Calculation of Chemistry Factors using R.E. Ginna, Turkey Point & Davis Besse Surveillance Capsule Data

Material	Capsule	Capsule f[a]	FF[b]	ΔRT_{NDT}[c]	$FF*\Delta RT_{NDT}$	FF^2
Lower Shell Forging 125P666	V	0.587	0.851	25	21.275	0.724
	R	1.02	1.006	25	25.150	1.012
	T	1.69	1.144	30	34.320	1.309
	S	3.64	1.335	42	56.070	1.782
				SUM:	136.815	4.827
	$CF_{LSF\ 125P666} = \Sigma(FF * RT_{NDT}) \div \Sigma(FF^2) = (136.815) \div (4.827) =$ **28.3°F**					
Intermediate Shell Forging 125S255	V	0.587	0.851	0	0	0.724
	R	1.02	1.006	0	0	1.012
	T	1.69	1.144	0	0	1.309
	S	3.64	1.335	60	80.1	1.782
				SUM:	80.1	4.827
	$CF_{ISF\ 125S255} = \Sigma(FF * RT_{NDT}) \div \Sigma(FF^2) = (80.1) \div (4.827) =$ **16.6°F**					
Ginna Surveillance Weld Metal (Heat # 61782)	V	0.587	0.851	149.8 (140)	127.480	0.724
	R	1.02	1.006	176.6 (165)	177.660	1.012
	T	1.69	1.144	160.5 (150)	183.612	1.309
	S	3.64	1.335	219.4 (205)	292.899	1.782
				SUM:	781.651	4.827
	$CF_{Ht.\ \#\ 61782} = \Sigma(FF * RT_{NDT}) \div \Sigma(FF^2) = (781.651) \div (4.827) =$ **161.9°F**					
Turkey Point Surveillance Weld Material[d] (Heat # 71249)	Davis	2.956	1.287	221 (215)	284.427	1.656
	T (TP3)	0.699	0.900	163 (166)	146.700	0.810
	V (TP3)	1.484	1.109	176 (179)	195.184	1.230
	T(TP4)	0.673	0.889	208 (211)	184.912	0.790
				SUM:	811.223	4.486
	$CF_{Ht\ \#\ 71249} = \Sigma(FF * RT_{NDT}) \div \Sigma(FF^2) = (811.223°F) \div (4.486) =$ **180.8°F**					

See Next Page for Notes

Notes:

(a) f = fluence. See Table 3, (x 10^{19} n/cm^2, E > 1.0 MeV).

(b) FF = fluence factor = $f^{(0.28 - 0.1 * \log f)}$.

(c) ΔRT_{NDT} values are the measured 30 ft-lb shift values taken from the following documents:
- Ginna Plate and Weld... WCAP-14684[9].
- Turkey Point & Davis Besse... WCAP-15092 R.3[7].

(d) Ginna operates with an average inlet temperature of approximately 549°F, Turkey Point 3&4 operate with an average inlet temperature of approximately 546°F, and Davis Besse operates with an average inlet temperature of approximately 555°F. The measured ΔRT_{NDT} values from the Turkey Point 3&4 surveillance program were adjusted by subtracting 3°F to each measured ΔRT_{NDT} and the Davis Besse surveillance program data was adjusted by adding 6°F to the measured ΔRT_{NDT} value before applying the ratio procedure. The surveillance weld metal ΔRT_{NDT} values have been adjusted by a ratio factor of:
Ratio Ginna = 1.07, Ratio Turkey Point = 1.0 (conservative), Ratio Davis Besse = 1.0 (conservative)
The pre-adjusted values are in parenthesis.

TABLE 5
Summary of the R.E. Ginna Reactor Vessel Beltline Material Chemistry Factors

Material	Chemistry Factor	
	Position 1.1	Position 2.1
Nozzle Shell Forging 123P118	44.0°F	- - -
Intermediate Shell Forging 125S255	44.0°F	16.6°F
Lower Shell Forging 125P666	31.0°F	28.3°F
Nozzle to Intermediate Shell Girth Weld (Heat # 71249)	167.6°F	180.8°F[a]
Intermediate Shell to Lower Shell Girth Weld (Heat # 61782)	170.4°F	161.9°F
Ginna Surveillance Weld Seams (Heat # 61782)	158.9°F	- - -

(a) Using Surveillance Data from Turkey Point.

3 RADIATION ANALYSIS AND NEUTRON DOSIMETRY

3.1 INTRODUCTION

This section describes a discrete ordinates S_n transport analysis performed for the R. E. Ginna reactor to determine the neutron radiation environment within the reactor pressure vessel and surveillance capsules. In this evaluation, fast neutron exposure parameters in terms of fast neutron fluence (E > 1.0 MeV) and iron atom displacements (dpa) were established on a plant and fuel cycle specific basis for the first twenty nine reactor operating cycles. In addition, neutron dosimetry sensor sets from the first four surveillance capsules withdrawn from the R. E. Ginna reactor were re-analyzed using current dosimetry evaluation methodology. The results of these dosimetry re-evaluations provided a validation of the plant specific neutron transport calculations. The validated calculations were then used to project future fluence accumulation through operating periods extending to 54 effective full power years (efpy).

The use of fast neutron fluence (E > 1.0 MeV) to correlate measured material property changes to the neutron exposure of the material has traditionally been accepted for development of damage trend curves as well as for the implementation of trend curve data to assess vessel condition. In recent years, however, it has been suggested that an exposure model that accounts for differences in neutron energy spectra between surveillance capsule locations and positions within the vessel wall could lead to an improvement in the uncertainties associated with damage trend curves as well as to a more accurate evaluation of damage gradients through the reactor vessel wall.

Because of this potential shift away from a threshold fluence toward an energy dependent damage function for data correlation, ASTM Standard Practice E853, "Analysis and Interpretation of Light-Water Reactor Surveillance Results," recommends reporting displacements per iron atom (dpa) along with fluence (E > 1.0 MeV) to provide a data base for future reference. The energy dependent dpa function to be used for this evaluation is specified in ASTM Standard Practice E693, "Characterizing Neutron Exposures in Iron and Low Alloy Steels in Terms of Displacements per Atom." The application of the dpa parameter to the assessment of embrittlement gradients through the thickness of the reactor vessel wall has already been promulgated in Revision 2 to Regulatory Guide 1.99, "Radiation Embrittlement of Reactor Vessel Materials." Therefore, in keeping with the philosophy espoused in the current standards governing pressure vessel exposure evaluations, dpa data is also included in this section.

All of the calculations and dosimetry evaluations described in this report were based on the latest available nuclear cross-section data derived from ENDF/B-VI and made use of the latest available calculational tools. Furthermore, the neutron transport and dosimetry evaluation methodologies follow the guidance and meet the requirements of Regulatory Guide 1.190, "Calculational and Dosimetry Methods for Determining Pressure Vessel Neutron Fluence."[11] Additionally, the methods used to determine the pressure vessel neutron exposure are consistent with the NRC approved methodology described in WCAP-14040-NP-A, "Methodology Used to Develop Cold Overpressure Mitigating System Setpoints and RCS Heatup and Cooldown Limit Curves," January 1996.[2]

3.2 NEUTRON TRANSPORT CALCULATIONS

In performing the fast neutron exposure evaluations for the R. E. Ginna surveillance capsules and reactor vessel, plant specific forward transport calculations were carried out using the following three-dimensional flux synthesis technique:

$$\phi(r,\theta,z) = \phi(r,\theta) * \frac{\phi(r,z)}{\phi(r)}$$

where $\phi(r,\theta,z)$ is the synthesized three-dimensional neutron flux distribution, $\phi(r,\theta)$ is the transport solution in r,θ geometry, $\phi(r,z)$ is the two-dimensional solution for a cylindrical reactor model using the actual axial core power distribution, and $\phi(r)$ is the one-dimensional solution for a cylindrical reactor model using the same source per unit height as that used in the r,θ two-dimensional calculation.

For the R. E. Ginna analysis, all of the transport calculations were carried out using the DORT two-dimensional discrete ordinates code Version 3.1[13] and the BUGLE-96 cross-section library[14]. The BUGLE-96 library provides a 67 group coupled neutron-gamma ray cross-section data set produced specifically for light water reactor application. In these analyses, anisotropic scattering was treated with a P_5 legendre expansion and the angular discretization was modeled with an S_{16} order of angular quadrature.

A plan view of the r,θ model of the R. E. Ginna reactor geometry at the core midplane is shown in Figure 1. Since the reactor exhibits octant symmetry only a 0° to 45° sector is depicted. In addition to the core, reactor internals, pressure vessel and primary biological shield, the model also included explicit representations of the surveillance capsules, the pressure vessel cladding, and the insulation located external to the pressure vessel.

From a neutronic standpoint the inclusion of the surveillance capsules and associated support structure in the analytical model is significant. Since the presence of the capsules and structure has a marked impact on the magnitude of the neutron flux as well as on the relative neutron and gamma ray spectra at dosimetry locations within the capsules, a meaningful evaluation of the radiation environment internal to the capsules can be made only when these perturbation effects are properly accounted for in the analysis.

In developing the r,θ analytical model of the reactor geometry shown in Figure 1, nominal design dimensions were employed for the various structural components. Likewise, water temperatures and, hence, coolant density in the reactor core and downcomer regions of the reactor were taken to be representative of full power operating conditions. The reactor core itself was treated as a homogeneous mixture of fuel, cladding, water, and miscellaneous core structures such as fuel assembly grids, guide tubes, etc. The r,θ geometric mesh description of the reactor model shown in Figure 3.2-1 consisted of 170 radial by 67 azimuthal intervals. Mesh sizes were chosen to assure that proper convergence of the inner iterations was achieved on a pointwise basis. The pointwise inner iteration flux convergence criterion utilized in the r,θ calculations was set at a value of 0.001.

A section view of the r,z model of the R. E. Ginna reactor is shown in Figure 2. The model extended radially from the centerline of the reactor core out to a location interior to the primary biological shield and over an axial span from an elevation 1 foot below the active fuel to approximately 1 foot above the active fuel. As in the case of the r,θ model, nominal design dimensions and full power coolant densities were

employed in the calculations. In this case, the homogenous core region was treated as an equivalent cylinder with a volume equal to that of the active core zone. The stainless steel former plates located between the core baffle and core barrel regions were also explicitly included in the model. The r,z geometric mesh description of the reactor model shown in Figure 2 consisted of 153 radial by 90 axial intervals. Mesh sizes were chosen to assure that proper convergence of the inner iterations was achieved on a pointwise basis. The pointwise inner iteration flux convergence criterion utilized in the r,z calculations was also set at a value of 0.001.

The one-dimensional radial model used in the synthesis procedure consisted of the same 153 radial mesh intervals included in the r,z model. Thus, radial synthesis factors could easily be determined on a meshwise basis throughout the entire geometry.

The core power distributions used in the plant specific transport analysis for the R. E. Ginna reactor were taken from the appropriate fuel cycle design reports for Cycles 1 through 29. The data extracted from the design reports represented cycle average relative assembly powers, burnups, and axial distributions. Therefore, the calculated results provided data in terms of fuel cycle averaged neutron flux which, when multiplied by the appropriate fuel cycle length, in turn, yielded the incremental fast neutron exposure for each fuel cycle. In constructing, the core source distributions, the energy distribution of the source was based on an appropriate fission split for uranium and plutonium isotopes; and from that fission split, composite values of energy release per fission, neutron yield per fission, and fission spectrum were determined. Fluence projections beyond the end of Cycle 29 were based on the assumption that the core power distribution averaged over Cycles 26 through 29 would be representative of future plant operation. Cycles 26 through 29 were designed as 18 month fuel cycles using the low leakage fuel management concept.

The maximum calculated fast neutron fluence (E > 1.0 MeV) and dpa exposure values for the R. E. Ginna pressure vessel are provided in Table 6. As presented, these data represent the maximum exposure of the pressure vessel clad/base metal interface at azimuthal angles of 0, 15, 30, and 45 degrees relative to the core cardinal axes. The data tabulation includes the plant specific calculated fluence at the end of cycle twenty nine (the last cycle completed at the R. E. Ginna plant) and projections for future operation to 28, 32, 36, 40, 44, 48, 52, and 54 EFPY. Similar data applicable to the intermediate shell to nozzle shell circumferential weld as well as to the nozzle shell course located above the top of the active fuel stack are given in Table 7.

The results of the updated fluence calculations for the four surveillance capsules withdrawn to date from the R. E. Ginna reactor are provided in Table 8. These calculated values of neutron fluence should be used to specify the neutron exposure of the irradiated test specimens for use in materials damage correlations.

Updated lead factors for the R. E. Ginna surveillance capsules are provided in Table 9. The capsule lead factor is defined as the ratio of the calculated fluence at the geometric center of the surveillance capsule to the corresponding maximum calculated fluence at the pressure vessel clad/base metal interface.

In Table 9, the lead factors for capsules that have been withdrawn from the reactor (V, R, T, and S) were based on the calculated fluence values for the irradiation period corresponding to the time of withdrawal for the individual capsules. For the capsules remaining in the reactor (P and N), the lead factors correspond to the calculated fluence values at the projected end of cycle twenty nine, the last fuel cycle completed at the time of analysis. The lead factors provided in Table 9 should be used as the basis for the development of future capsule withdrawal schedules for the R. E. Ginna reactor.

Figure 1
R. E. Ginna r,θ Reactor Geometry at the Core Midplane

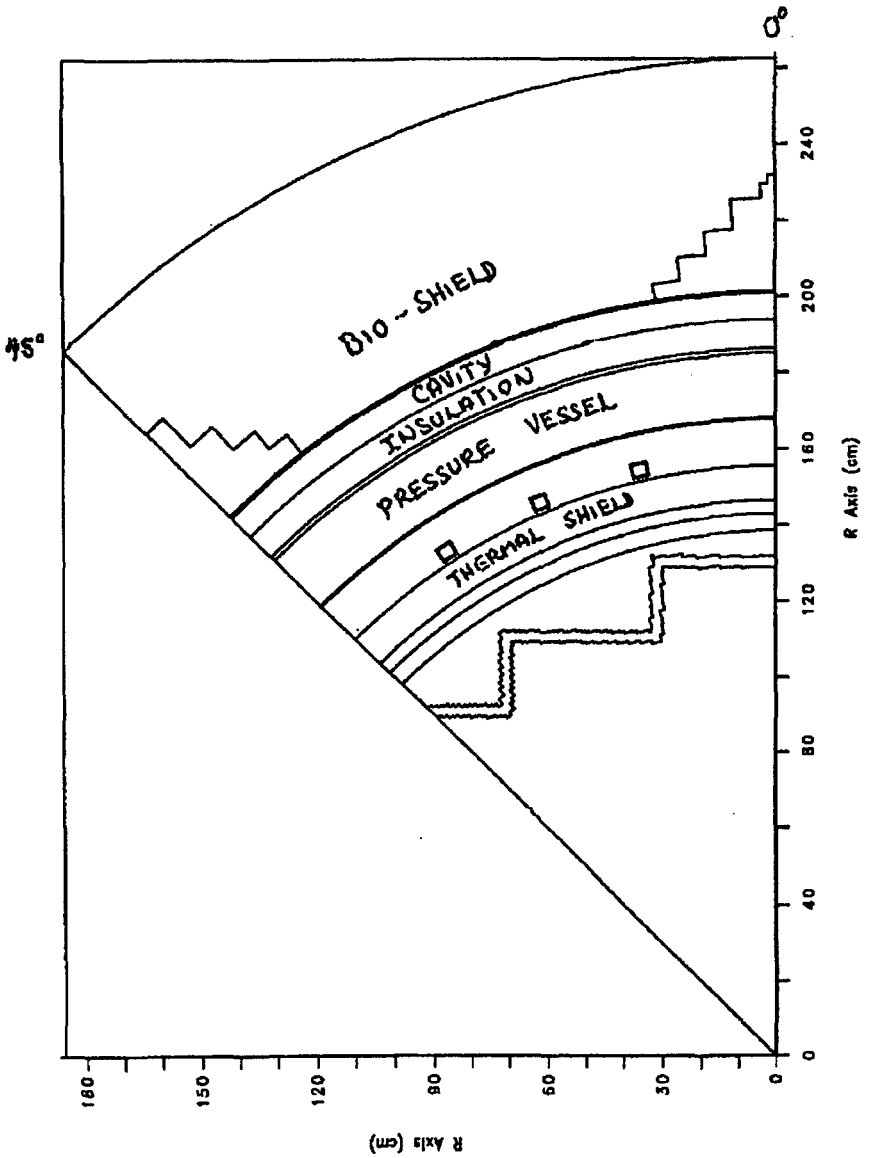

Figure 2
R. E. Ginna r,z Geometry

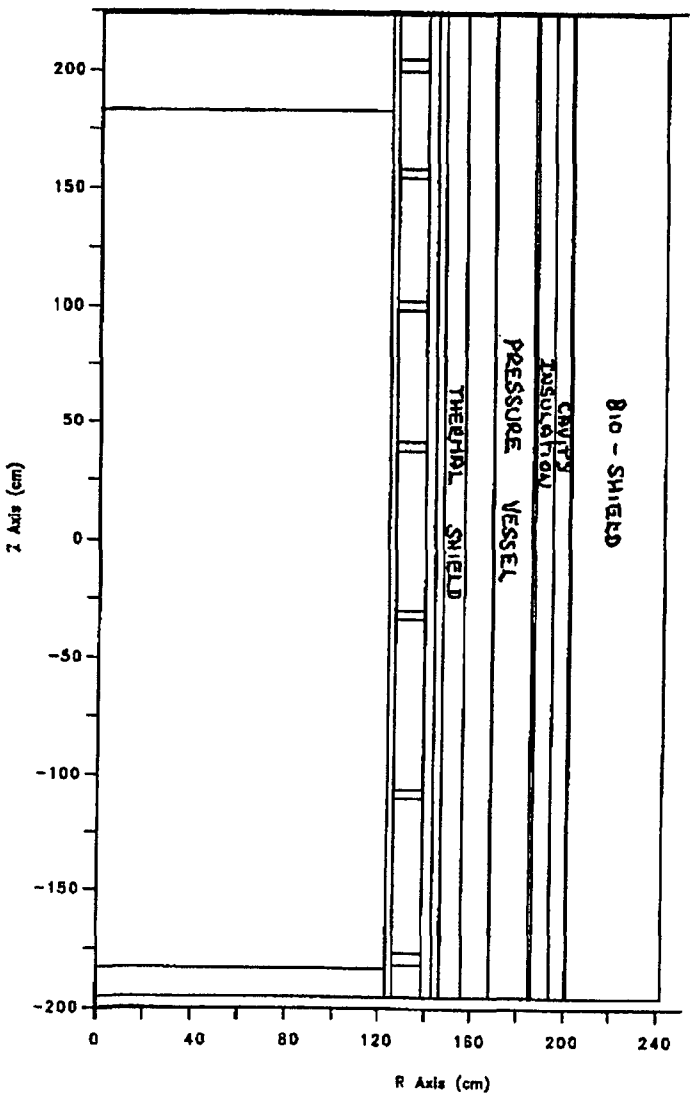

Table 6
Summary of Calculated Maximum Pressure Vessel Exposure
Clad/Base Metal Interface

Neutron Fluence [E > 1.0 MeV]

Cumulative Operating Time [EFPY]	Neutron Fluence [n/cm^2]			
	0.0 Degrees	15.0 Degrees	30.0 Degrees	45.0 Degrees
24.8 (EOC 29)	2.68e+19	1.69e+19	1.22e+19	1.09e+19
28	2.94e+19	1.85e+19	1.34e+19	1.20e+19
32	3.26e+19	2.05e+19	1.48e+19	1.33e+19
36	3.57e+19	2.25e+19	1.63e+19	1.46e+19
40	3.89e+19	2.45e+19	1.77e+19	1.60e+19
44	4.21e+19	2.65e+19	1.92e+19	1.73e+19
48	4.53e+19	2.85e+19	2.07e+19	1.86e+19
52	4.85e+19	3.05e+19	2.21e+19	2.00e+19
54	5.01e+19	3.15e+19	2.28e+19	2.06e+19

Iron Atom Displacements

Cumulative Operating Time [EFPY]	Iron Atom Displacements [dpa]			
	0.0 Degrees	15.0 Degrees	30.0 Degrees	45.0 Degrees
24.8 (EOC 29)	4.37e-02	2.85e-02	2.01e-02	1.77e-02
28	4.79e-02	3.12e-02	2.20e-02	1.94e-02
32	5.31e-02	3.46e-02	2.44e-02	2.16e-02
36	5.82e-02	3.79e-02	2.68e-02	2.37e-02
40	6.34e-02	4.12e-02	2.91e-02	2.59e-02
44	6.86e-02	4.46e-02	3.15e-02	2.80e-02
48	7.38e-02	4.79e-02	3.39e-02	3.02e-02
52	7.89e-02	5.12e-02	3.63e-02	3.23e-02
54	8.15e-02	5.29e-02	3.75e-02	3.34e-02

Table 7

Summary of Calculated Maximum Exposure of the Intermediate to Nozzle Shell Circumferential Weld and the Nozzle Shell Course Clad/Base Metal Interface

Neutron Fluence [E > 1.0 MeV]

Cumulative Operating Time [EFPY]	Neutron Fluence [n/cm^2]			
	0.0 Degrees	15.0 Degrees	30.0 Degrees	45.0 Degrees
24.8 (EOC 29)	1.05e+18	6.64e+17	4.78e+17	4.26e+17
28	1.16e+18	7.28e+17	5.25e+17	4.68e+17
32	1.28e+18	8.07e+17	5.83e+17	5.21e+17
36	1.41e+18	8.86e+17	6.41e+17	5.74e+17
40	1.54e+18	9.65e+17	6.98e+17	6.27e+17
44	1.66e+18	1.04e+18	7.56e+17	6.80e+17
48	1.79e+18	1.12e+18	8.14e+17	7.32e+17
52	1.92e+18	1.20e+18	8.72e+17	7.85e+17
54	1.98e+18	1.24e+18	9.00e+17	8.12e+17

Iron Atom Displacements

Cumulative Operating Time [EFPY]	Iron Atom Displacements [dpa]			
	0.0 Degrees	15.0 Degrees	30.0 Degrees	45.0 Degrees
24.8 (EOC 29)	1.83e-03	1.19e-03	8.38e-04	7.35e-04
28	2.01e-03	1.31e-03	9.20e-04	8.09e-04
32	2.23e-03	1.45e-03	1.02e-03	9.01e-04
36	2.45e-03	1.59e-03	1.12e-03	9.92e-04
40	2.67e-03	1.73e-03	1.22e-03	1.08e-03
44	2.89e-03	1.87e-03	1.33e-03	1.17e-03
48	3.11e-03	2.02e-03	1.43e-03	1.27e-03
52	3.33e-03	2.16e-03	1.53e-03	1.36e-03
54	3.44e-03	2.23e-03	1.58e-03	1.40e-03

Table 8
Calculated Surveillance Capsule Exposure

Capsule	Irradiation Time [EFPY]	Fluence (E > 1.0 MeV) [n/cm^2]	Iron Displacements [dpa]
V	1.4	5.87e+18	1.07e-02
R	2.6	1.02e+19	1.85e-02
T	6.9	1.69e+19	2.94e-02
S	17.0	3.64e+19	6.38e-02

Table 9
Calculated Surveillance Capsule Lead Factors

Capsule ID And Location	Status	Lead Factor
V (13°)	Withdrawn EOC 1	2.96
R (13°)	Withdrawn EOC 3	2.97
T (23°)	Withdrawn EOC 9	1.82
S (33°)	Withdrawn EOC 22	1.79
P (23°)	In Reactor	1.91
N (33°)	In Reactor	1.81

Note: Lead factors for capsules remaining in the reactor are based on cycle specific exposure calculations through fuel cycle twenty nine.

3.3 NEUTRON DOSIMETRY EVALUATIONS

3.3.1 Sensor Reaction Rate Determinations

In this section, the results of the evaluations of the four neutron sensor sets withdrawn as a part of the R. E. Ginna Reactor Vessel Materials Surveillance Program are presented. The capsule designation, location within the reactor, and time of withdrawal of each of these dosimetry sets were as follows:

Capsule ID	Azimuthal Location	Withdrawal Time	Irradiation Time [efps]
V	13°	End of Cycle 1	4.46e+07
R	13°	End of Cycle 3	8.05e+07
T	23°	End of Cycle 9	2.17e+08
S	33°	End of Cycle 22	5.36e+08

The type and radial locations of the neutron sensors within the capsules are summarized as follows:

Sensor Type	**Radius [cm]**
Copper	158.11
Iron – Core Side Charpy	158.11
Iron – Vessel Side Charpy	159.11
Nickel	158.91
Uranium 238	158.35
Neptunium 237	158.35
Bare Cobalt-Aluminum	159.11
Cd Cov. Cobalt-Aluminum	159.11

The copper, nickel, and cobalt-aluminum monitors, in wire form, were placed in holes drilled in spacers at several axial levels within the capsules. The cadmium shielded uranium and neptunium fission monitors were accommodated within the dosimeter block located near the center of the capsule. The iron sensors were obtained by cutting small samples from individual charpy specimens taken from several locations within the surveillance capsules.

The use of passive monitors such as those listed above does not yield a direct measure of the energy dependent neutron flux at the point of interest. Rather, the activation or fission process is a measure of the integrated effect that the time and energy dependent neutron flux has on the target material over the course of the irradiation period. An accurate assessment of the average neutron flux level incident on the various monitors may be derived from the activation measurements only if the irradiation parameters are well known. In particular, the following variables are of interest:

- The measured specific activity of each monitor,
- The physical characteristics of each monitor,
- The operating history of the reactor,
- The energy response of each monitor, and
- The neutron energy spectrum at the monitor location.

The radiometric counting of each of the R. E. Ginna dosimetry data sets was accomplished by Westinghouse using established ASTM procedures. Following sample preparation and weighing, the activity of each monitor was determined by means of a high resolution gamma spectrometer. For the copper, iron, nickel, and cobalt-aluminum sensors, these analyses were performed by direct counting of each of the individual samples. In the case of the uranium and neptunium fission sensors, the analyses were carried out by direct counting preceded by disolution and chemical separation of cesium from the sensor material.

The irradiation history of the reactor over the irradiation period experienced by Capsules V, R, T, and S was obtained on a monthly basis from reactor startup to the end of the dosimetry evaluation period. For the sensor sets utilized in the surveillance capsules, the half-lives of the product isotopes are long enough that a monthly histogram describing reactor operation has proven to be an adequate representation for use in radioactive decay corrections for the reactions of interest in the exposure evaluations.

Having the measured specific activities, the operating history of the reactor, and the physical characteristics of the sensors, reaction rates referenced to full power operation were determined from the following equation:

$$R = \frac{A}{N_o F Y \sum_{j=1}^{n} \frac{P_j}{P_{ref}} C_j (1 - e^{-\lambda t_j}) e^{\lambda t_d}}$$

where:

A	=	measured specific activity (dps/g)
R	=	reaction rate averaged over the irradiation period and referenced to operation at a core power level of P_{ref} (rps/nucleus).
N_0	=	number of target element atoms per gram of sensor.

F	=	weight fraction of the target isotope in the sensor material.
Y	=	number of product atoms produced per reaction.
P_j	=	average core power level during irradiation period j (MW).
P_{ref}	=	maximum or reference core power level of the reactor (MW).
C_j	=	calculated ratio of $\phi(E \geq 1.0$ MeV) during irradiation period j to the time weighted average $\phi(E \geq 1.0$ MeV) over the entire irradiation period.
λ	=	decay constant of the product isotope (s^{-1}).
t_j	=	length of irradiation period j (s).
t_d	=	decay time following irradiation period j (s).

and the summation is carried out over the total number of monthly intervals comprising the irradiation period.

In the above equation, the ratio P_j/P_{ref} accounts for month by month variation of power level within a given fuel cycle. The ratio C_j is calculated for each fuel cycle using the methodology described in Section 3.2 of this report and accounts for the change in sensor reaction rates caused by variations in flux level due to changes in core power spatial distributions from fuel cycle to fuel cycle. For a single cycle irradiation C_j = 1.0. However, for multiple cycle irradiations, particularly those employing low leakage fuel management, the additional C_j correction must be utilized. This additional correction can be quite significant for sensor sets that have been irradiated for many fuel cycles in a reactor that has transitioned from non-low leakage to low leakage fuel management.

Prior to using the measured reaction rates in the least squares adjustment procedure discussed later in this section, additional corrections were made to U^{238} measurements to account for the presence of U^{235} impurities in the sensors as well as to adjust for the build-in of plutonium isotopes over the course of the irradiation. These corrections were location and fluence dependent and were derived from the plant specific discrete ordinates analysis described in Section 3.2. Corrections were also made to the U^{238} and Np^{237} sensor reaction rates to account for gamma ray induced fission reactions that occurred over the course of the irradiation. These photo-fission corrections were, likewise, location dependent and were based on the transport calculations described in Section 3.2.

Results of the sensor reaction rate determinations for Capsules V, R, T, and S are given in Tables 10 through 14. In Tables 10 through 13, the measured specific activities, gradient corrected specific activities, and decay corrected reaction rates are listed for Capsules V, R, T, and S, respectively. A summary of the reaction rates for each capsule is provided in Table 14. The data listed in Table 14 are indexed to the geometric center of the respective capsules and included all corrections for U^{235} impurities, Pu build-in, and photo-fission effects.

Table 10
Measured Sensor Specific Activities and Reaction Rates
Capsule V

Sample ID	Foil ID	Radius [cm.]	Measured Activity [dps/g]	Saturated Activity [dps/g]	Radially Adjusted Saturated Activity [dps/g]	Radially Adjusted Reaction Rate [rps/atom]	Average Reaction Rate [rps/atom]
CU	Top	158.11	7.38E+04	4.63E+05	4.43E+05	6.77E-17	
CU	Top-Mid	158.11	6.77E+04	4.25E+05	4.07E+05	6.21E-17	
CU	Bot-Mid	158.11	7.48E+04	4.70E+05	4.49E+05	6.86E-17	
CU	Bottom	158.11	8.13E+04	5.10E+05	4.89E+05	7.45E-17	6.82E-17
FE	W-1	158.11	2.47E+06	5.00E+06	4.82E+06	7.64E-15	
FE	R-1	158.11	2.57E+06	5.20E+06	5.02E+06	7.95E-15	
FE	S-6	158.11	2.18E+06	4.41E+06	4.25E+06	6.74E-15	
FE	P-7	158.11	2.57E+06	5.20E+06	5.02E+06	7.95E-15	
FE	W-2	159.11	2.04E+06	4.13E+06	4.78E+06	7.58E-15	
FE	R-3	159.11	1.95E+06	3.95E+06	4.57E+06	7.25E-15	
FE	S-8	159.11	2.02E+06	4.09E+06	4.74E+06	7.51E-15	
FE	P-9	159.11	2.10E+06	4.25E+06	4.92E+06	7.80E-15	7.55E-15
NI	Middle	158.11	2.38E+07	6.51E+07	6.21E+07	8.90E-15	8.90E-15
U	Middle	158.35	2.30E+05	7.26E+06	7.26E+06	4.77E-14	3.91E-14
NP	Middle	158.35	1.23E+06	3.88E+07	3.88E+07	2.48E-13	2.44E-13

Notes:

- The average U-238(n,f) reaction rate of 2.91E-14 includes the correction of a factor of 0.861 to account for plutonium build-in and an additional factor of 0.950 to account for photo-fission effects in the sensor.
- The average Np-237(n,f) reaction rate of 2.44E-13 includes the correction of a factor of 0.983 to account for the photo-fission effects in the sensor.

Table 11
Measured Sensor Specific Activities and Reaction Rates
Capsule R

Sample ID	Foil ID	Radius [cm.]	Measured Activity [dps/g]	Saturated Activity [dps/g]	Radially Adjusted Saturated Activity [dps/g]	Radially Adjusted Reaction Rate [rps/atom]	Average Reaction Rate [rps/atom]
74-2204	Top	158.11	1.08E+05	4.42E+05	4.23E+05	6.45E-17	
74-2207	Top-Mid	158.11	9.68E+04	3.96E+05	3.79E+05	5.78E-17	
74-2213	Bot-Mid	158.11	1.15E+05	4.70E+05	4.50E+05	6.87E-17	
74-2216	Bottom	158.11	1.15E+05	4.70E+05	4.50E+05	6.87E-17	6.49E-17
74-2202	W-13	158.11	2.08E+06	5.19E+06	5.00E+06	7.93E-15	
74-2200	R-14	158.11	1.98E+06	4.94E+06	4.76E+06	7.55E-15	
74-2198	P-18	158.11	2.06E+06	5.14E+06	4.95E+06	7.85E-15	
74-2203	W-14	159.11	1.63E+06	4.07E+06	4.71E+06	7.46E-15	
74-2201	R-15	159.11	1.70E+06	4.24E+06	4.91E+06	7.78E-15	
74-2199	P-19	159.11	1.85E+06	4.61E+06	5.34E+06	8.47E-15	7.84E-15
74-2210	Middle	158.11	5.83E+06	7.36E+07	7.03E+07	1.01E-14	1.01E-14
74-2220	Middle	158.35	4.32E+05	7.79E+06	7.79E+06	5.12E-14	4.11E-14
74-2219	Middle	158.35	4.25E+06	7.66E+07	7.66E+07	4.89E-13	4.81E-13
74-2205	Top	159.11	3.09E+07	1.26E+08	1.22E+08	7.97E-12	
74-2208	Top-Mid	159.11	3.14E+07	1.28E+08	1.24E+08	8.10E-12	
74-2211	Middle	159.11	2.96E+07	1.21E+08	1.17E+08	7.64E-12	
74-2214	Bot-Mid	159.11	2.94E+07	1.20E+08	1.16E+08	7.59E-12	
74-2217	Bottom	159.11	2.94E+07	1.20E+08	1.16E+08	7.59E-12	7.78E-12
74-2206	Top	159.11	1.19E+07	4.87E+07	5.69E+07	3.71E-12	
74-2209	Top-Mid	159.11	1.18E+07	4.83E+07	5.64E+07	3.68E-12	
74-2212	Middle	159.11	1.07E+07	4.38E+07	5.11E+07	3.34E-12	
74-2215	Bot-Mid	159.11	1.24E+07	5.07E+07	5.92E+07	3.87E-12	
74-2218	Bottom	159.11	1.24E+07	5.07E+07	5.92E+07	3.87E-12	3.69E-12

Notes:

- The average U-238(n,f) reaction rate of 4.11E-14 includes the correction of a factor of 0.845 to account for plutonium build-in and an additional factor of 0.950 to account for photo-fission effects in the sensor.
- The average Np-237(n,f) reaction rate of 4.81E-13 includes the correction of a factor of 0.983 to account for the photo-fission effects in the sensor.

Table 12
Measured Sensor Specific Activities and Reaction Rates
Capsule T

Sample ID	Foil ID	Radius [cm.]	Measured Activity [dps/g]	Saturated Activity [dps/g]	Radially Adjusted Saturated Activity [dps/g]	Radially Adjusted Reaction Rate [rps/atom]	Average Reaction Rate [rps/atom]
81-1392	Top	158.11	1.60E+05	3.51E+05	3.35E+05	5.11E-17	
81-1395	Top-Mid	158.11	1.40E+05	3.07E+05	2.93E+05	4.47E-17	
81-1402	Bot-Mid	158.11	1.66E+05	3.64E+05	3.48E+05	5.30E-17	
81-1415	Bottom	158.11	1.74E+05	3.82E+05	3.64E+05	5.56E-17	5.11E-17
81-3390	S-22	158.11	1.14E+06	3.36E+06	3.19E+06	5.06E-15	
81-3392	P-28	158.11	1.27E+06	3.74E+06	3.56E+06	5.64E-15	
81-3394	W-21	158.11	1.30E+06	3.83E+06	3.64E+06	5.77E-15	
81-3391	S-23	159.11	1.01E+06	2.97E+06	3.43E+06	5.44E-15	
81-3393	P-29	159.11	1.03E+06	3.03E+06	3.50E+06	5.55E-15	
81-3395	W-22	159.11	1.10E+06	3.24E+06	3.74E+06	5.92E-15	5.56E-15
81-1399	Middle	158.11	8.62E+05	5.25E+07	5.01E+07	7.17E-15	7.17E-15
81-1388	Middle	158.35	7.41E+05	5.34E+06	5.34E+06	3.51E-14	2.74E-14
81-1389	Middle	158.35	6.09E+06	4.39E+07	4.39E+07	2.80E-13	2.75E-13
81-1390	Top	159.11	3.17E+07	6.96E+07	6.60E+07	4.31E-12	
81-1393	Top-Mid	159.11	3.06E+07	6.72E+07	6.37E+07	4.16E-12	
81-1396	Middle	159.11	3.03E+07	6.65E+07	6.31E+07	4.12E-12	
81-1400	Bot-Mid	159.11	3.27E+07	7.18E+07	6.81E+07	4.44E-12	
81-1403	Bottom	159.11	3.07E+07	6.74E+07	6.39E+07	4.17E-12	4.24E-12
81-1391	Top	159.11	1.21E+07	2.66E+07	3.06E+07	2.00E-12	
81-1394	Top-Mid	159.11	1.13E+07	2.48E+07	2.86E+07	1.87E-12	
81-1397	Middle	159.11	1.16E+07	2.55E+07	2.94E+07	1.92E-12	
81-1401	Bot-Mid	159.11	1.26E+07	2.77E+07	3.19E+07	2.08E-12	
81-1404	Bottom	159.11	1.20E+07	2.63E+07	3.04E+07	1.98E-12	1.97E-12

Notes:

- The average U-238(n,f) reaction rate of 2.74E-14 includes the correction of a factor of 0.820 to account for plutonium build-in and an additional factor of 0.955 to account for photo-fission effects in the sensor.
- The average Np-237(n,f) reaction rate of 2.75E-13 includes the correction of a factor of 0.984 to account for the photo-fission effects in the sensor.

Table 13
Measured Sensor Specific Activities and Reaction Rates
Capsule S

Sample ID	Foil ID	Radius [cm.]	Measured Activity [dps/g]	Saturated Activity [dps/g]	Radially Adjusted Saturated Activity [dps/g]	Radially Adjusted Reaction Rate [rps/atom]	Average Reaction Rate [rps/atom]
93-3163	Top	158.11	2.06E+05	3.06E+05	2.92E+05	4.45E-17	
93-3166	Top-Mid	158.11	1.82E+05	2.70E+05	2.58E+05	3.93E-17	
93-3172	Bot-Mid	158.11	1.98E+05	2.94E+05	2.81E+05	4.28E-17	
93-3175	Bottom	158.11	2.18E+05	3.24E+05	3.09E+05	4.71E-17	4.34E-17
93-4326	P-31	158.11	1.62E+06	2.93E+06	2.79E+06	4.42E-15	4.42E-15
93-3169	Middle	158.11	8.51E+06	4.27E+07	4.06E+07	5.81E-15	5.81E-15
93-3159	Middle	158.35	1.40E+06	4.63E+06	4.63E+06	3.04E-14	2.19E-14
93-3160	Middle	158.35	1.11E+07	3.67E+07	3.67E+07	2.34E-13	2.30E-13
93-3161	Top	159.11	3.55E+07	5.27E+07	5.05E+07	3.29E-12	
93-3164	Top-Mid	159.11	3.71E+07	5.51E+07	5.28E+07	3.44E-12	
93-3167	Middle	159.11	3.39E+07	5.03E+07	4.82E+07	3.15E-12	
93-3170	Bot-Mid	159.11	3.60E+07	5.35E+07	5.12E+07	3.34E-12	
93-3173	Bottom	159.11	3.45E+07	5.12E+07	4.91E+07	3.20E-12	3.29E-12
93-3162	Top	159.11	1.43E+07	2.12E+07	2.47E+07	1.61E-12	
93-3165	Top-Mid	159.11	1.37E+07	2.03E+07	2.37E+07	1.54E-12	
93-3168	Middle	159.11	1.31E+07	1.95E+07	2.26E+07	1.48E-12	
93-3171	Bot-Mid	159.11	1.45E+07	2.15E+07	2.50E+07	1.63E-12	
93-3174	Bottom	159.11	1.35E+07	2.00E+07	2.33E+07	1.52E-12	1.56E-12

Notes:

- The average U-238(n,f) reaction rate of 2.19E-14 includes the correction of a factor of 0.755 to account for plutonium build-in and an additional factor of 0.953 to account for photo-fission effects in the sensor.
- The average Np-237(n,f) reaction rate of 2.30E-13 includes the correction of a factor of 0.983 to account for the photo-fission effects in the sensor.

Table 14
Summary of Sensor Reaction Rates from Capsules V, R, T, and S

	Measured Reaction Rate [rps/nucleus]			
Sensor Reaction	**Capsule V**	**Capsule R**	**Capsule T**	**Capsule S**
Cu-63(n,α)Co-60	6.82e-17	6.49e-17	5.11e-17	4.34e-17
Fe-54(n,p)Mn-54	7.55e-15	7.84e-15	5.56e-15	4.42e-15
Ni-58(n,p)Co-58	8.90e-15	1.01e-14	7.17e-15	5.81e-15
U-238(n,f)Cs-137 Cd Covered	3.91e-14	4.11e-14	2.74e-14	2.19e-14
Np-237(n,f)Cs-137 Cd Covered	**Rejected**	4.81e-13	2.75e-13	2.30e-13
Co-59(n,γ) Co-60	None	7.78e-12	4.24e-12	3.29e-12
Co-59(n,γ) Co-60 Cd Covered	None	3.69e-12	1.97e-12	1.56e-12

3.4 LEAST SQUARES EVALUATION OF SENSOR SETS

Least squares adjustment methods provide the capability of combining the measurement data with the neutron transport calculation resulting in a Best Estimate neutron energy spectrum with associated uncertainties. Best Estimates for key exposure parameters such as $\phi(E > 1.0\ MeV)$ or dpa/s along with their uncertainties are then easily obtained from the adjusted spectrum. In general, the least squares methods, as applied to surveillance capsule dosimetry evaluations, act to reconcile the measured sensor reaction rate data, dosimetry reaction cross-sections, and the calculated neutron energy spectrum within their respective uncertainties. For example,

$$R_i \pm \delta_{R_i} = \sum_g (\sigma_{ig} \pm \delta_{\sigma_{ig}})(\phi_g \pm \delta_{\phi_g})$$

relates a set of measured reaction rates, R_i, to a single neutron spectrum, ϕ_g, through the multigroup dosimeter reaction cross-section, σ_{ig}, each with an uncertainty δ. The primary objective of the least squares evaluation is to produce unbiased estimates of the neutron exposure parameters at the location of the measurement.

For the least squares evaluation of the R. E. Ginna surveillance capsule dosimetry, The FERRET code[15] was employed to combine the results of the plant specific neutron transport calculations and sensor set reaction rate measurements to determine best estimate values of exposure parameters ($\phi(E > 1.0\ MeV)$ and dpa) along with associated uncertainties for the three in-vessel capsules withdrawn to date.

The application of the least squares methodology requires the following input:

1 - The calculated neutron energy spectrum and associated uncertainties at the measurement location.

2 - The measured reaction rates and associated uncertainty for each sensor contained in the multiple foil set.

3 - The energy dependent dosimetry reaction cross-sections and associated uncertainties for each sensor contained in the multiple foil sensor set.

For the R. E. Ginna application, the calculated neutron spectrum was obtained from the results of plant specific neutron transport calculations described in Section 3.2 of this report. The sensor reaction rates were derived from the measured specific activities using the procedures described in Section 3.3. The dosimetry reaction cross-sections and uncertainties were obtained from the SNLRML dosimetry cross-section library[16]. The SNLRML library is an evaluated dosimetry reaction cross-section compilation recommended for use in LWR evaluations by ASTM Standard E1018, "Application of ASTM Evaluated Cross-Section Data File, Matrix E 706 (IIB)".

The uncertainties associated with the measured reaction rates, dosimetry cross-sections, and calculated neutron spectrum were input to the least squares procedure in the form of variances and covariances. The assignment of the input uncertainties followed the guidance provided in ASTM Standard E 944, "Application of Neutron Spectrum Adjustment Methods in Reactor Surveillance.

The following provides a summary of the uncertainties associated with the least squares evaluation of the R. E. Ginna surveillance capsule sensor sets:

Reaction Rate Uncertainties

The overall uncertainty associated with the measured reaction rates includes components due to the basic measurement process, the irradiation history corrections, and the corrections for competing reactions. A high level of accuracy in the reaction rate determinations is assured by utilizing laboratory procedures that conform to the ASTM National Consensus Standards for reaction rate determinations for each sensor type.

After combining all of these uncertainty components, the sensor reaction rates derived from the counting and data evaluation procedures were assigned the following net uncertainties for input to the least squares evaluation:

Reaction	Uncertainty
$Cu^{63}(n,\alpha)Co^{60}$	5%
$Fe^{54}(n,p)Mn^{54}$	5%
$Ni^{58}(n,p)Co^{58}$	5%
$U^{238}(n,f)Cs^{137}$	10%
$Np^{237}(n,f)Cs^{137}$	10%
$Co^{59}(n,\gamma)Co^{60}$	5%

Dosimetry Cross-Section Uncertainties

The reaction rate cross-sections used in the least squares evaluations were taken from the SNLRML library. This data library provides reaction cross-sections and associated uncertainties, including covariances, for 66 dosimetry sensors in common use. Both cross-sections and uncertainties are provided in a fine multigroup structure for use in least squares adjustment applications. These cross-sections were compiled from the most recent cross-section evaluations and they have been tested with respect to their accuracy and consistency for least squares evaluations. Further, the library has been empirically tested for use in fission spectra determination as well as in the fluence and energy characterization of 14 MeV neutron sources. Detailed discussions of the contents of the SNLRML library along with the evaluation process for each of the sensors is provided in Reference 16.

For sensors included in the R. E. Ginna surveillance capsules, the following uncertainties in the fission spectrum averaged cross-sections are provided in the SNLRML documentation package.

Reaction	Uncertainty
$Cu^{63}(n,\alpha)Co^{60}$	4.08-4.16%
$Fe^{54}(n,p)Mn^{54}$	3.05-3.11%
$Ni^{58}(n,p)Co^{58}$	4.49-4.56%
$U^{238}(n,f)Cs^{137}$	0.54-0.64%
$Np^{237}(n,f)Cs^{137}$	10.32-10.97%
$Co^{59}(n,\gamma)Co^{60}$	0.79-3.59%

These tabulated ranges provide an indication of the dosimetry cross-section uncertainties associated with the sensor sets used in LWR irradiations.

Calculated Neutron Spectrum

The neutron spectrum input to the least squares adjustment procedure was obtained directly from the results of plant specific transport calculations for each surveillance capsule location. The spectrum at each location was input in an absolute sense (rather than as simply a relative spectral shape). Therefore, within the constraints of the assigned uncertainties, the calculated data were treated equally with the measurements.

While the uncertainties associated with the reaction rates were obtained from the measurement procedures and counting benchmarks and the dosimetry cross-section uncertainties were supplied directly with the SNLRML library, the uncertainty matrix for the calculated spectrum was constructed from the following relationship:

$$M_{g'g} = R_n^2 + R_g * R_{g'} * P_{g'g}$$

where R_n specifies an overall fractional normalization uncertainty and the fractional uncertainties $R_{g'}$ and R_g specify additional random groupwise uncertainties that are correlated with a correlation matrix given by:

$$P_{g'g} = [1 - \vartheta] * \delta_{g'g} + \vartheta * e^{-H}$$

where

$$H = \frac{(g - g')^2}{2\gamma^2}$$

The first term in the correlation matrix equation specifies purely random uncertainties, while the second term describes the short range correlations over a group range γ (θ specifies the strength of the latter term). The value of δ is 1.0 when g = g' and 0.0 otherwise.

The set of parameters defining the input covariance matrix for the R. E. Ginna calculated spectra was as follows:

Flux Normalization Uncertainty (R_n)	15%
Flux Group Uncertainties (R_g, $R_{g'}$)	
(E > 0.0055 MeV)	15%
(0.68 eV < E < 0.0055 MeV)	29%
(E < 0.68 eV)	52%
Short Range Correlation (θ)	
(E > 0.0055 MeV)	0.9
(0.68 eV < E < 0.0055 MeV)	0.5
(E < 0.68 eV)	0.5
Flux Group Correlation Range (γ)	
(E > 0.0055 MeV)	6
(0.68 eV < E < 0.0055 MeV)	3
(E < 0.68 eV)	2

Results of the least squares evaluation of the four sensor sets withdrawn from the R. E. Ginna reactor are provided in Tables 15 and 16. In Table 15, measured, calculated, and best estimate sensor reaction rates are given for Capsules V, R, T, and S. The improvement in the fit of the adjusted spectra to the measurements is evident for all four capsule data sets. Prior to the application of the adjustment procedure M/C ratios for individual foil reactions ranged from 0.75 to 1.32, while after the adjustment M/BE ratios ranged from 0.91 to 1.12. Thus, demonstrating a significant improvement in the data fits.

In Table 16, the calculated and best estimate exposure rates and integrated exposures of Capsules V, R, T, and S are given. Data are provided in terms of both fluence (E > 1.0 MeV) and iron atom displacements.

Table 15
Comparison of Measured, Calculated, and Best Estimate
Reaction Rates at the Surveillance Capsule Center

Surveillance Capsule V

Reaction	Reaction Rate [rps/atom]			M/C	M/BE
	Measured	Calculated	Best Estimate		
$Cu^{63}(n,\alpha)Co^{60}$	6.82e-17	6.69e-17	6.54e-17	1.02	1.04
$Fe^{54}(n,p)Mn^{54}$	7.55e-15	8.14e-15	7.34e-15	0.93	1.03
$Ni^{58}(n,p)Co^{58}$	8.90e-15	1.14e-14	9.74e-15	0.78	0.91
$U^{238}(n,f)Cs^{137}$ Cd	3.91e-14	4.37e-14	3.77e-14	0.89	1.04
$Np^{237}(n,f)Cs^{137}$ Cd					
$Co^{59}(n,\gamma)Co^{60}$					
$Co^{59}(n,\gamma)Co^{60}$ Cd					

Surveillance Capsule R

Reaction	Reaction Rate [rps/atom]			M/C	M/BE
	Measured	Calculated	Best Estimate		
$Cu^{63}(n,\alpha)Co^{60}$	6.49e-17	6.41e-17	6.39e-17	1.01	1.02
$Fe^{54}(n,p)Mn^{54}$	7.84e-15	7.79e-15	7.74e-15	1.01	1.01
$Ni^{58}(n,p)Co^{58}$	1.01e-14	1.09e-14	1.06e-14	0.93	0.95
$U^{238}(n,f)Cs^{137}$ Cd	4.11e-14	4.18e-14	4.22e-14	0.98	0.97
$Np^{237}(n,f)Cs^{137}$ Cd	4.81e-13	3.64e-13	4.28e-13	1.32	1.12
$Co^{59}(n,\gamma)Co^{60}$	7.78e-12	9.22e-12	7.84e-12	0.84	0.99
$Co^{59}(n,\gamma)Co^{60}$ Cd	3.69e-12	3.66e-12	3.68e-12	1.01	1.00

Surveillance Capsule T

Reaction	Reaction Rate [rps/atom]			M/C	M/BE
	Measured	Calculated	Best Estimate		
$Cu^{63}(n,\alpha)Co^{60}$	5.11e-17	5.09e-17	5.05e-17	1.00	1.01
$Fe^{54}(n,p)Mn^{54}$	5.56e-15	5.51e-15	5.51e-15	1.01	1.01
$Ni^{58}(n,p)Co^{58}$	7.17e-15	7.58e-15	7.46e-15	0.95	0.96
$U^{238}(n,f)Cs^{137}$ Cd	2.74e-14	2.70e-14	2.76e-14	1.01	0.99
$Np^{237}(n,f)Cs^{137}$ Cd	2.75e-13	2.14e-13	2.49e-13	1.29	1.10
$Co^{59}(n,\gamma)Co^{60}$	4.24e-12	5.01e-12	4.27e-12	0.85	0.99
$Co^{59}(n,\gamma)Co^{60}$ Cd	1.97e-12	1.89e-12	1.96e-12	1.04	1.01

Table 15 (continued)

Comparison of Measured, Calculated, and Best Estimate
Reaction Rates at the Surveillance Capsule Center

Surveillance Capsule S

Reaction	Reaction Rate [rps/atom]			M/C	M/BE
	Measured	Calculated	Best Estimate		
$Cu^{63}(n,\alpha)Co^{60}$	4.34e-17	4.25e-17	4.21e-17	1.02	1.03
$Fe^{54}(n,p)Mn^{54}$	4.42e-15	4.66e-15	4.45e-15	0.95	0.99
$Ni^{58}(n,p)Co^{58}$	5.81e-15	6.43e-15	6.05e-15	0.90	0.96
$U^{238}(n,f)Cs^{137}$ Cd	2.19e-14	2.33e-14	2.24e-14	0.94	0.98
$Np^{237}(n,f)Cs^{137}$ Cd	2.30e-13	1.88e-13	2.06e-13	1.22	1.12
$Co^{59}(n,\gamma)Co^{60}$	3.29e-12	4.36e-12	3.32e-12	0.75	0.99
$Co^{59}(n,\gamma)Co^{60}$ Cd	1.56e-12	1.70e-12	1.56e-12	0.92	1.00

Table 16
Comparison of Calculated and Best Estimate
Exposure Parameters at the Surveillance Capsule Center

Time Averaged Exposure Rates

	$\phi(E > 1.0\ MeV)$ [n/cm^2-s]			
	Calculated	Best Estimate	Uncertainty	BE/C
Capsule V	1.32e+11	1.13e+11	7%	0.86
Capsule R	1.26e+11	1.30e+11	6%	1.03
Capsule T	7.79e+10	8.11e+10	6%	1.04
Capsule S	6.78e+10	6.62e+10	6%	0.98

	Iron Atom Displacements [dpa/s]			
	Calculated	Best Estimate	Uncertainty	BE/C
Capsule V	2.40e-10	2.05e-10	9%	0.86
Capsule R	2.30e-10	2.37e-10	7%	1.03
Capsule T	1.36e-10	1.40e-10	7%	1.03
Capsule S	1.19e-10	1.16e-10	7%	0.97

Integrated Capsule Exposure

	$\Phi\ (E > 1.0\ MeV)$ [n/cm^2]			
	Calculated	Best Estimate	Uncertainty	BE/C
Capsule V	5.87e+18	5.03e+18	7%	0.86
Capsule R	1.02e+19	1.05e+19	6%	1.03
Capsule T	1.69e+19	1.76e+19	6%	1.04
Capsule S	3.64e+19	3.55e+19	6%	0.98

	Iron Atom Displacements [dpa]			
	Calculated	Best Estimate	Uncertainty	BE/C
Capsule V	1.07e-02	9.15e-03	9%	0.86
Capsule R	1.85e-02	1.91e-02	7%	1.03
Capsule T	2.94e-02	3.04e-02	7%	1.03
Capsule S	6.38e-02	6.22e-02	7%	0.97

3.5 COMPARISON OF MEASUREMENTS AND CALCULATIONS

In this section, comparisons of the measurement results from the four surveillance capsules withdrawn to date with the corresponding analytical predictions at the measurement locations are provided. These comparisons are given on two levels. In the first instance, calculations of individual sensor reaction rates are compared directly with the corresponding values obtained from the measured specific activities. In the second case, calculations of fast neutron exposure rates in terms of $\phi(E > 1.0$ MeV) and dpa/s are compared with the best estimate results obtained from the least squares evaluation of the three capsule dosimetry results. These two levels of comparison yield consistent and similar results with all measurement to calculation comparisons falling within the 20% limits specified as the acceptance criteria in Regulatory Guide 1.190.

In the case of the direct comparison of measured and calculated sensor reaction rates, the M/C comparisons for fast neutron reactions range from 0.78–1.32 for the 19 samples included in the data set. In the comparisons of best estimate and calculated fast neutron exposure parameters, the corresponding BE/C comparisons range from 0.85 –1.04 for the four surveillance capsules withdrawn to date.

Based on these comparisons, it is concluded that the data comparisons validate the use of the calculated fast neutron exposures provided in Section 3.2 of this report for use in the assessment of the condition of the materials comprising the beltline region of the R. E. Ginna reactor pressure vessel.

Table 17
Comparison of Measured and Calculated Neutron Sensor Reaction Rates
For In-Vessel Surveillance Capsules V, R, T, and S

Capsule	M/C Ratio					Average	% std dev
	Cu-63(n,α)	Fe-54(n,p)	Ni-58(n,p)	U-238(n,f)	Np-237(n,f)		
V	1.02	0.93	0.78	0.89		0.91	10.9
R	1.01	1.01	0.93	0.98	1.32	1.05	14.8
T	1.00	1.01	0.95	1.01	1.29	1.05	12.7
S	1.02	0.95	0.90	0.94	1.22	1.01	12.7
Average	1.01	0.97	0.89	0.96	1.28	**1.01**	**13.3**
% std dev	0.8	4.2	8.4	5.5	3.9		

Note: The average and % std dev values in bold face type represent the average and standard deviation of the entire 19 sample threshold foil data set.

Table 18
Comparison of Best Estimate and Calculated Fast Neutron Exposure Rates
For In-Vessel Surveillance Capsules V, R, T, and S

Capsule	BE/C Ratio	
	Neutron Fluence	Iron Atom Displacements
V	0.86	0.86
R	1.03	1.03
T	1.04	1.03
S	0.98	0.97
Average	0.98	0.97
% std dev	8.7	8.6

4 CRITERIA FOR ALLOWABLE PRESSURE-TEMPERATURE RELATIONSHIPS

4.1 OVERALL APPROACH

The ASME approach for calculating the allowable limit curves for various heatup and cooldown rates specifies that the total stress intensity factor, K_I, for the combined thermal and pressure stresses at any time during heatup or cooldown cannot be greater than the reference stress intensity factor, K_{Ic}, for the metal temperature at that time. K_{Ic} is obtained from the reference fracture toughness curve, defined in Code Case N-640, "Alternative Reference Fracture Toughness for Development of PT Limit Curves for Section XI"[3 & 4] of the ASME Appendix G to Section XI. The K_{Ic} curve is given by the following equation:

$$K_{Ic} = 33.2 + 20.734 * e^{[0.02(T - RT_{NDT})]} \quad (1)$$

where,

K_{Ic} = reference stress intensity factor as a function of the metal temperature T and the metal reference nil-ductility temperature RT_{NDT}

This K_{Ic} curve is based on the lower bound of static critical K_I values measured as a function of temperature on specimens of SA-533 Grade B Class1, SA-508-1, SA-508-2, SA-508-3 steel.

4.2 METHODOLOGY FOR PRESSURE-TEMPERATURE LIMIT CURVE DEVELOPMENT

The governing equation for the heatup-cooldown analysis is defined in Appendix G of the ASME Code as follows:

$$C^* K_{Im} + K_{It} < K_{Ic} \quad (2)$$

where,

K_{Im} = stress intensity factor caused by membrane (pressure) stress

K_{It} = stress intensity factor caused by the thermal gradients

K_{Ic} = function of temperature relative to the RT_{NDT} of the material

C = 2.0 for Level A and Level B service limits

C = 1.5 for hydrostatic and leak test conditions during which the reactor core is not critical

For membrane tension, the corresponding K_I for the postulated defect is:

$$K_{Im} = M_m \times (pR_i / t) \tag{3}$$

where, M_m for an inside surface flaw is given by:

M_m = 1.85 for $\sqrt{t} < 2$,

M_m = $0.926\sqrt{t}$ for $2 \leq \sqrt{t} \leq 3.464$,

M_m = 3.21 for $\sqrt{t} > 3.464$

Similarly, M_m for an outside surface flaw is given by:

M_m = 1.77 for $\sqrt{t} < 2$,

M_m = $0.893\sqrt{t}$ for $2 \leq \sqrt{t} \leq 3.464$,

M_m = 3.09 for $\sqrt{t} > 3.464$

and p = internal pressure, Ri = vessel inner radius, and t = vessel wall thickness.

For bending stress, the corresponding K_I for the postulated defect is:

K_{Ib} = M_b * Maximum Stress, where M_b is two-thirds of M_m

The maximum K_I produced by radial thermal gradient for the postulated inside surface defect of G-2120 is $K_{It} = 0.953 \times 10^{-3} \times CR \times t^{2.5}$, where CR is the cooldown rate in °F/hr., or for a postulated outside surface defect, $K_{It} = 0.753 \times 10^{-3} \times HU \times t^{2.5}$, where HU is the heatup rate in °F/hr.

The through-wall temperature difference associated with the maximum thermal K_I can be determined from Fig. G-2214-1. The temperature at any radial distance from the vessel surface can be determined from Fig. G-2214-2 for the maximum thermal K_I.

(a) The maximum thermal K_I relationship and the temperature relationship in Fig. G-2214-1 are applicable only for the conditions given in G-2214.3(a)(1) and (2).

(b) Alternatively, the K_I for radial thermal gradient can be calculated for any thermal stress distribution and at any specified time during cooldown for a ¼-thickness inside surface defect using the relationship:

$$K_{It} = (1.0359C_0 + 0.6322C_1 + 0.4753C_2 + 0.3855C_3) * \sqrt{\pi a} \tag{4}$$

or similarly, K_{IT} during heatup for a ¼-thickness outside surface defect using the relationship:

$$K_{It} = (1.043C_0 + 0.630C_1 + 0.481C_2 + 0.401C_3) * \sqrt{\pi a} \quad (5)$$

where the coefficients C_0, C_1, C_2 and C_3 are determined from the thermal stress distribution at any specified time during the heatup or cooldown using the form:

$$\sigma(x) = C_0 + C_1(x/a) + C_2(x/a)^2 + C_3(x/a)^3 \quad (6)$$

and x is a variable that represents the radial distance from the appropriate (i.e., inside or outside) surface to any point on the crack front and a is the maximum crack depth.

Note, that equations 3, 4 and 5 were implemented in the OPERLIM computer code, which is the program used to generate the pressure-temperature (P-T) limit curves. No other changes were made to the OPERLIM computer code with regard to P-T calculation methodology. Therefore, the P-T curve methodology is unchanged from that described in WCAP-14040, "Methodology used to Develop Cold Overpressure Mitigating System Setpoints and RCS Heatup and Cooldown Limit Curves"[2] Section 2.6 (equations 2.6.2-4 and 2.6.3-1) with the exceptions just described above.

At any time during the heatup or cooldown transient, K_{Ic} is determined by the metal temperature at the tip of a postulated flaw at the 1/4T and 3/4T location, the appropriate value for RT_{NDT}, and the reference fracture toughness curve. The thermal stresses resulting from the temperature gradients through the vessel wall are calculated and then the corresponding (thermal) stress intensity factors, K_{It}, for the reference flaw are computed. From Equation 2, the pressure stress intensity factors are obtained and, from these, the allowable pressures are calculated.

For the calculation of the allowable pressure versus coolant temperature during cooldown, the reference flaw of Appendix G to the ASME Code is assumed to exist at the inside of the vessel wall. During cooldown, the controlling location of the flaw is always at the inside of the wall because the thermal gradients produce tensile stresses at the inside, which increase with increasing cooldown rates. Allowable pressure-temperature relations are generated for both steady-state and finite cooldown rate situations. From these relations, composite limit curves are constructed for each cooldown rate of interest.

The use of the composite curve in the cooldown analysis is necessary because control of the cooldown procedure is based on the measurement of reactor coolant temperature, whereas the limiting pressure is actually dependent on the material temperature at the tip of the assumed flaw. During cooldown, the 1/4T vessel location is at a higher temperature than the fluid adjacent to the vessel inner diameter. This condition, of course, is not true for the steady-state situation. It follows that, at any given reactor coolant temperature, the ΔT (temperature) developed during cooldown results in a higher value of K_{Ic} at the 1/4T location for finite cooldown rates than for steady-state operation. Furthermore, if conditions exist so that the increase in K_{Ic} exceeds K_{It}, the calculated allowable pressure during cooldown will be greater than the steady-state value.

The above procedures are needed because there is no direct control on temperature at the 1/4T location and, therefore, allowable pressures may unknowingly be violated if the rate of cooling is decreased at various intervals along a cooldown ramp. The use of the composite curve eliminates this problem and ensures conservative operation of the system for the entire cooldown period.

Three separate calculations are required to determine the limit curves for finite heatup rates. As is done in the cooldown analysis, allowable pressure-temperature relationships are developed for steady-state conditions as well as finite heatup rate conditions assuming the presence of a 1/4T defect at the inside of the wall. The heatup results in compressive stresses at the inside surface that alleviate the tensile stresses produced by internal pressure. The metal temperature at the crack tip lags the coolant temperature; therefore, the K_{Ic} for the 1/4T crack during heatup is lower than the K_{Ic} for the 1/4T crack during steady-state conditions at the same coolant temperature. During heatup, especially at the end of the transient, conditions may exist so that the effects of compressive thermal stresses and lower K_{Ic} values do not offset each other, and the pressure-temperature curve based on steady-state conditions no longer represents a lower bound of all similar curves for finite heatup rates when the 1/4T flaw is considered. Therefore, both cases have to be analyzed in order to ensure that at any coolant temperature the lower value of the allowable pressure calculated for steady-state and finite heatup rates is obtained.

The second portion of the heatup analysis concerns the calculation of the pressure-temperature limitations for the case in which a 1/4T flaw located at the 1/4T location from the outside surface is assumed. Unlike the situation at the vessel inside surface, the thermal gradients established at the outside surface during heatup produce stresses which are tensile in nature and therefore tend to reinforce any pressure stresses present. These thermal stresses are dependent on both the rate of heatup and the time (or coolant temperature) along the heatup ramp. Since the thermal stresses at the outside are tensile and increase with increasing heatup rates, each heatup rate must be analyzed on an individual basis.

Following the generation of pressure-temperature curves for both the steady-state and finite heatup rate situations, the final limit curves are produced by constructing a composite curve based on a point-by-point comparison of the steady-state and finite heatup rate data. At any given temperature, the allowable pressure is taken to be the lesser of the three values taken from the curves under consideration. The use of the composite curve is necessary to set conservative heatup limitations because it is possible for conditions to exist wherein, over the course of the heatup ramp, the controlling condition switches from the inside to the outside, and the pressure limit must at all times be based on analysis of the most critical criterion.

4.3 CLOSURE HEAD/VESSEL FLANGE REQUIREMENTS

10 CFR Part 50, Appendix G[5] addresses the metal temperature of the closure head flange and vessel flange regions. This rule states that the metal temperature of the closure flange regions must exceed the material unirradiated RT_{NDT} by at least 120°F for normal operation when the pressure exceeds 20 percent of the preservice hydrostatic test pressure (3106 psi), which is 621 psig for R.E. Ginna. The limiting unirradiated RT_{NDT} of -52°F occurs in the vessel flange of the R.E. Ginna reactor vessel, so the minimum allowable temperature of this region is 68°F at pressures greater than 621 psig. This limit is shown in Figures 6-1 and 6-2 wherever applicable.

5 CALCULATION OF ADJUSTED REFERENCE TEMPERATURE

From Regulatory Guide 1.99, Revision 2, the adjusted reference temperature (ART) for each material in the beltline region is given by the following expression:

$$ART = \text{Initial } RT_{NDT} + \Delta RT_{NDT} + \text{Margin} \quad (7)$$

Initial RT_{NDT} is the reference temperature for the unirradiated material as defined in paragraph NB-2331 of Section III of the ASME Boiler and Pressure Vessel Code[17]. If measured values of initial RT_{NDT} for the material in question are not available, generic mean values for that class of material may be used if there are sufficient test results to establish a mean and standard deviation for the class.

ΔRT_{NDT} is the mean value of the adjustment in reference temperature caused by irradiation and should be calculated as follows:

$$\Delta RT_{NDT} = CF * f^{(0.28 - 0.10 \log f)} \quad (8)$$

To calculate ΔRT_{NDT} at any depth (e.g., at 1/4T or 3/4T), the following formula must first be used to attenuate the fluence at the specific depth.

$$f_{(depth\ x)} = f_{surface} * e^{(-0.24x)} \quad (9)$$

where x inches (vessel beltline thickness is 6.5 inches) is the depth into the vessel wall measured from the vessel clad/base metal interface. The resultant fluence is then placed in Equation 8 to calculate the ΔRT_{NDT} at the specific depth.

The Westinghouse Radiation Engineering and Analysis Group evaluated the vessel fluence projections in Section 3 of this report. The evaluation used the ENDF/B-VI scattering cross-section data set. This is consistent with methods presented in WCAP-14040-NP-A, "Methodology Used to Develop Cold Overpressure Mitigating System Setpoints and RCS Heatup and Cooldown Limit Curves". Tables 6 and 7 contain the **calculated vessel surface fluences values** at various azimuthal locations, including the longitudinal location for the nozzle shell forging to intermediate shell forging girth weld. Tables 19 and 20 contain the 1/4T and 3/4T calculated fluences and fluence factors, per the Regulatory Guide 1.99, Revision 2, used to calculate the ART values for all beltline materials in the R.E. Ginna reactor vessel.

TABLE 19
Summary of the Vessel Surface, 1/4T and 3/4T Fluence Values
used for the Generation of the 52 EFPY Heatup/Cooldown Curves

Material	Surface (n/cm^2 ,E > 1.0 MeV)	1/4T (n/cm^2 ,E > 1.0 MeV)	3/4T (n/cm^2 ,E > 1.0 MeV)
Inter. & Lower Shell Forgings and the Inter. to Lower Shell Girth Weld (Peak Fluence)	4.85×10^{19}	3.28×10^{19}	1.51×10^{19}
Nozzle Shell Forging and the Nozzle to Inter. Shell Girth Weld	1.92×10^{18}	1.30×10^{18}	5.96×10^{17}

TABLE 20
Summary of the Calculated Fluence Factors used for the Generation of the 52 EFPY
Heatup and Cooldown Curves

Material	1/4T Fluence (n/cm^2 ,E > 1.0 MeV)	1/4T FF	3/4T Fluence (n/cm^2 ,E > 1.0 MeV)	3/4T FF
Inter. & Lower Shell Forgings and the Inter. to Lower Shell Girth Weld	3.28×10^{19}	1.31	1.51×10^{19}	1.11
Nozzle Shell Forging and the Nozzle to Inter. Shell Girth Weld	1.30×10^{18}	0.47	5.96×10^{17}	0.32

Margin is calculated as, $M = 2\sqrt{\sigma_i^2 + \sigma_\Delta^2}$. The standard deviation for the initial RT_{NDT} margin term, is σ_i 0°F when the initial RT_{NDT} is a measured value, and 17°F when a generic value is available. The standard deviation for the ΔRT_{NDT} margin term, σ_Δ, is 17°F for plates or forgings, and 8.5°F for plates or forgings when surveillance data is used. For welds, σ_Δ is equal to 28°F when surveillance capsule data is not used, and is 14°F (half the value) when credible surveillance capsule data is used. σ_Δ need not exceed 0.5 times the mean value of ΔRT_{NDT}.

Contained in Tables 21 and 22 are the calculations of the 52 EFPY ART values used for generation of the heatup and cooldown curves.

TABLE 21
Calculation of the ART Values for the 1/4T Location @ 52 EFPY

Material	RG 1.99 R2 Method	CF (°F)	FF	IRT_{NDT}[a] (°F)	ΔRT_{NDT} (°F)	Margin (°F)	ART[b] (°F)
Nozzle Shell Forging 123P118[a]	Position 1.1	44.0	0.47	30	20.7	20.7	71
Inter. Shell Forging 125S255	Position 1.1	44.0	1.31	20	57.6	34	**112**
	Position 2.1	16.6	1.31	20	21.7	34[c]	76
Lower Shell Forging 125P666	Position 1.1	31.0	1.31	40	40.6	34	115
	Position 2.1	28.3	1.31	40	37.1	17	94
Nozzle to Intermediate Shell Girth Weld (Heat # 71249)	Position 1.1	167.6	0.47	10	78.8	56	145
	Position 2.1	180.8	0.47	10	85.0	56[c]	151
Intermediate Shell to Lower Shell Girth Weld (Heat # 61782)	Position 1.1	170.4	1.31	-4.8	223.2	56	274
	Position 2.1	161.9	1.31	-4.8	212.1	48.3[d]	**256**

Notes:
(a) Initial RT_{NDT} values are measured values.
(b) ART = Initial RT_{NDT} + ΔRT_{NDT} + Margin (°F)
(c) Surveillance Data is not credible, thus the full σ_Δ is used in calculating the margin term.
(d) Based on Additional tests by B&W and documented in the Ginna PTLR…Used per the request of RGE.

TABLE 22
Calculation of the ART Values for the 3/4T Location @ 52 EFPY

Material	RG 1.99 R2 Method	CF (°F)	FF	IRT_{NDT}[a] (°F)	ΔRT_{NDT} (°F)	Margin (°F)	ART[b] (°F)
Nozzle Shell Forging 123P118[a]	Position 1.1	44.0	0.32	30	14.1	14.1	58
Inter. Shell Forging 125S255	Position 1.1	44.0	1.11	20	48.8	34	**103**
	Position 2.1	16.6	1.11	20	18.4	34[c]	72
Lower Shell Forging 125P666	Position 1.1	31.0	1.11	40	34.4	34	108
	Position 2.1	28.3	1.11	40	31.4	17	89
Nozzle to Intermediate Shell Girth Weld (Heat # 71249)	Position 1.1	167.6	0.32	10	53.6	53.6	117
	Position 2.1	180.8	0.32	10	57.9	56[c]	124
Intermediate Shell to Lower Shell Girth Weld (Heat # 61782)	Position 1.1	170.4	1.11	-4.8	189.1	56	240
	Position 2.1	161.9	1.11	-4.8	179.7	48.3[d]	**223**

Notes:
(a) Initial RT_{NDT} values are measured values.
(b) ART = Initial RT_{NDT} + ΔRT_{NDT} + Margin (°F)
(c) Surveillance Data is not credible, thus the full σ_Δ is used in calculating the margin term.
(d) Based on Additional tests by B&W and documented in the Ginna PTLR…Used per the request of RGE.

The upper to intermediate shell forging to lower shell forging girth weld has the highest overall ART. However, since Code Case N-641 allows for less restrictive methodology to be used when the highest ART comes from a girth weld, then the highest non-girth weld ART must be identified. The intermediate shell forging has the highest non-girth weld ART.

Contained in Table 23 is a summary of the limiting ARTs to be used in the generation of the R.E. Ginna reactor vessel heatup and cooldown curves. It has been determined based on the relief allowed via ASME Code Case N-641 (Circ. Flaw Methodology) and the magnitude of the girth weld ART values as compared to the intermediate shell forging ART values, that the intermediate shell forging ART values would produce a more conservative pressure temperature curve at the lower temperature portion of the curves. Thus, composite curves were created from two computer runs: 1) The highest "circ. flaw" ART with the "Circ. Flaw Methodology (ASME Code Case N-641), and 2) The highest "Axial Flaw" ART with the Axial Flaw (1996 ASME Code) Methodology. The limiting pressures and temperature were taken from both sets of curves to create the most limiting PT curves overall. These limiting curves will be presented in Section 6.

TABLE 23
Summary of the Limiting ART Values Used in the
Generation of the R.E. Ginna Heatup/Cooldown Curves

¼ T Limiting ART	¾ T Limiting ART
Intermediate to Lower Shell Girth Weld (*Limiting Circ. Flaw Material*)	
256	223
Intermediate Shell Forging (*Limiting Axial Flaw Material*)	
112	103

6 HEATUP AND COOLDOWN PRESSURE-TEMPERATURE LIMIT CURVES

Pressure-temperature limit curves for normal heatup and cooldown of the primary reactor coolant system have been calculated for the pressure and temperature in the reactor vessel beltline region using the methods discussed in Sections 4.0 and 5.0 of this report. This approved methodology is also presented in WCAP-14040-NP-A, Revision 2 with exception to those items discussed in Section 1 of this report.

Figure 3 presents the limiting heatup curves without margins for possible instrumentation errors using heatup rates of 60 and 100°F/hr applicable for the first 52 EFPY. These curves were generated using a combination of the1996 ASME Code Section XI, Appendix G with the limiting axial flaw ARTs and the ASME Code Case N-641 with the limiting circ. flaw ARTs. The limiting pressures and temperatures between the two cases produce a bounding heatup curves for the given rates. Figure 4 presents the limiting cooldown curves without margins for possible instrumentation errors using cooldown rates of 0, 20, 40, 60 and 100°F/hr applicable for 52 EFPY. Again, these curves were generated using a combination of the1996 ASME Code Section XI, Appendix G with the limiting axial flaw ARTs and the ASME Code Case N-641 with the limiting circ. flaw ARTs. Allowable combinations of temperature and pressure for specific temperature change rates are below and to the right of the limit line shown in Figures 3 and 4. This is in addition to other criteria, which must be met before the reactor is made critical, as discussed below in the following paragraphs.

The reactor must not be made critical until pressure-temperature combinations are to the right of the criticality limit line shown in Figure 3. The straight-line portion of the criticality limit is at the minimum permissible temperature for the 2485 psig inservice hydrostatic test as required by Appendix G to 10 CFR Part 50. The governing equation for the hydrostatic test is defined in Code Case N-641[3] (approved in February 1999) as follows:

$$1.5\ K_{Im} < K_{Ic}$$

where,

K_{Im} is the stress intensity factor covered by membrane (pressure) stress,

$K_{Ic} = 33.2 + 20.734\ e^{[0.02\,(T - RT_{NDT})]}$,

T is the minimum permissible metal temperature, and

RT_{NDT} is the metal reference nil-ductility temperature.

The criticality limit curve specifies pressure-temperature limits for core operation to provide additional margin during actual power production as specified in Reference 5. The pressure-temperature limits for core operation (except for low power physics tests) are that the reactor vessel must be at a temperature equal to or higher than the minimum temperature required for the inservice hydrostatic test, and at least 40°F higher than the minimum permissible temperature in the corresponding pressure-temperature curve for heatup and cooldown calculated as described in Section 4.0 of this report. For the heatup and cooldown curves without margins for instrumentation errors, the minimum temperatures for the in service hydrostatic leak tests for the R.E. Ginna reactor vessel at 52 EFPY is 162°F, respectively. The vertical line drawn from

these points on the pressure-temperature curve, intersecting a curve 40°F higher than the pressure-temperature limit curve constitutes the limit for core operation for the reactor vessel.

Figures 3 and 4 define all of the above limits for ensuring prevention of nonductile failure for the R.E. Ginna reactor vessel for 52 EFPY. The data points used for the heatup and cooldown pressure-temperature limit curves shown in Figures 3 and 4 are presented in Tables 24 and 25.

MATERIAL PROPERTY BASIS

LIMITING MATERIAL: INTER. to LOWER SHELL FORGING GIRTH WELD and INTER. SHELL FORGING
LIMITING ART VALUES AT 52 EFPY: 1/4T, 256°F (*Circ Flaw ART*), 112°F (*Axial Flaw ART*)
3/4T, 223°F (*Circ Flaw ART*), 103°F (*Axial Flaw ART*)

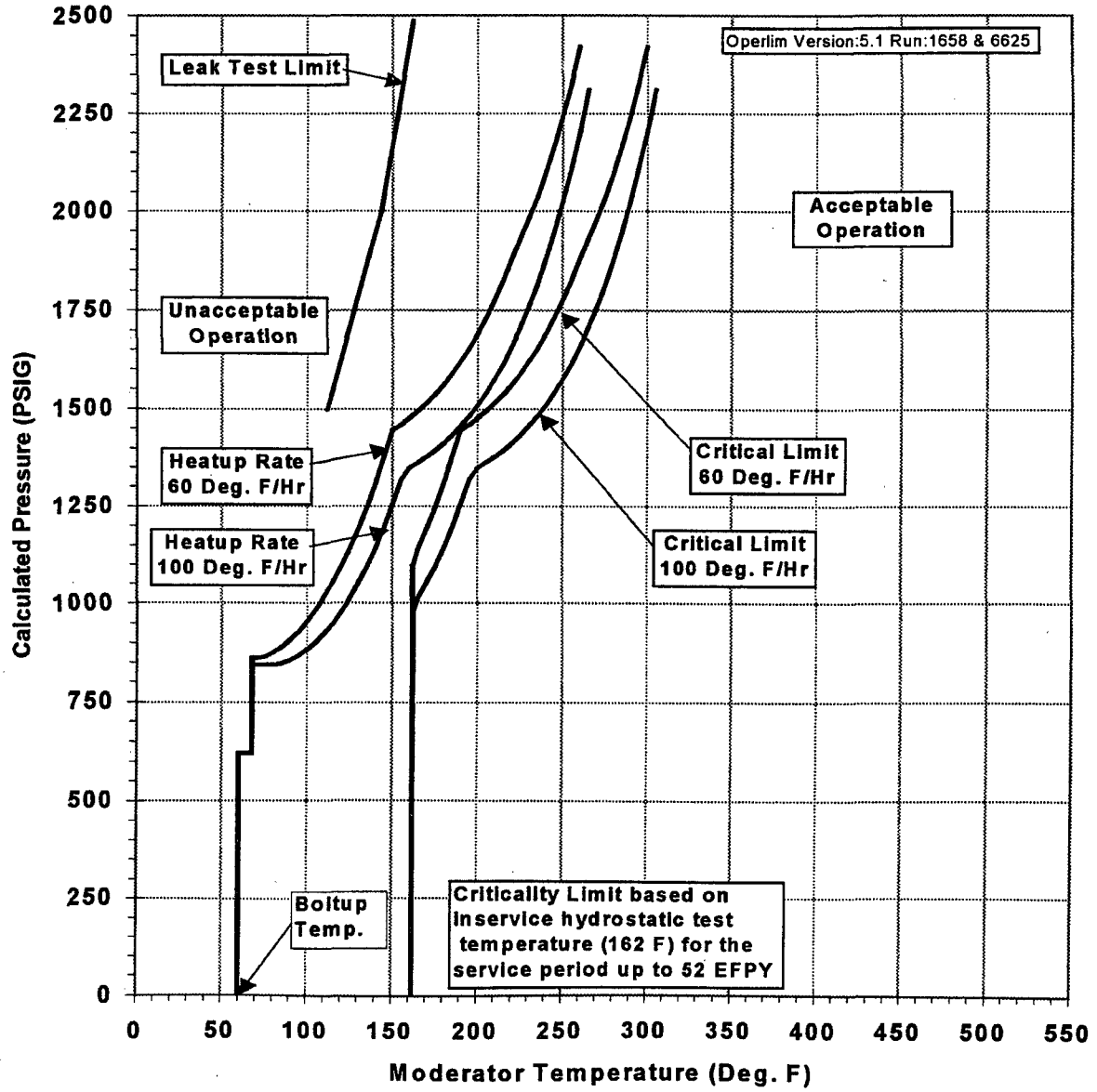

Figure 3 **R.E. Ginna Reactor Coolant System Heatup Limitations (Heatup Rates of 60 & 100°F/hr) Applicable for the First 52 EFPY (Without Margins for Instrumentation Errors) Using 1996 App.G Methodology**

MATERIAL PROPERTY BASIS

LIMITING MATERIAL: INTER. to LOWER SHELL FORGING GIRTH WELD and INTER. SHELL FORGING
LIMITING ART VALUES AT 52 EFPY: 1/4T, 256°F (*Circ Flaw ART*), 112°F (*Axial Flaw ART*)
3/4T, 223°F (*Circ Flaw ART*), 103°F (*Axial Flaw ART*)

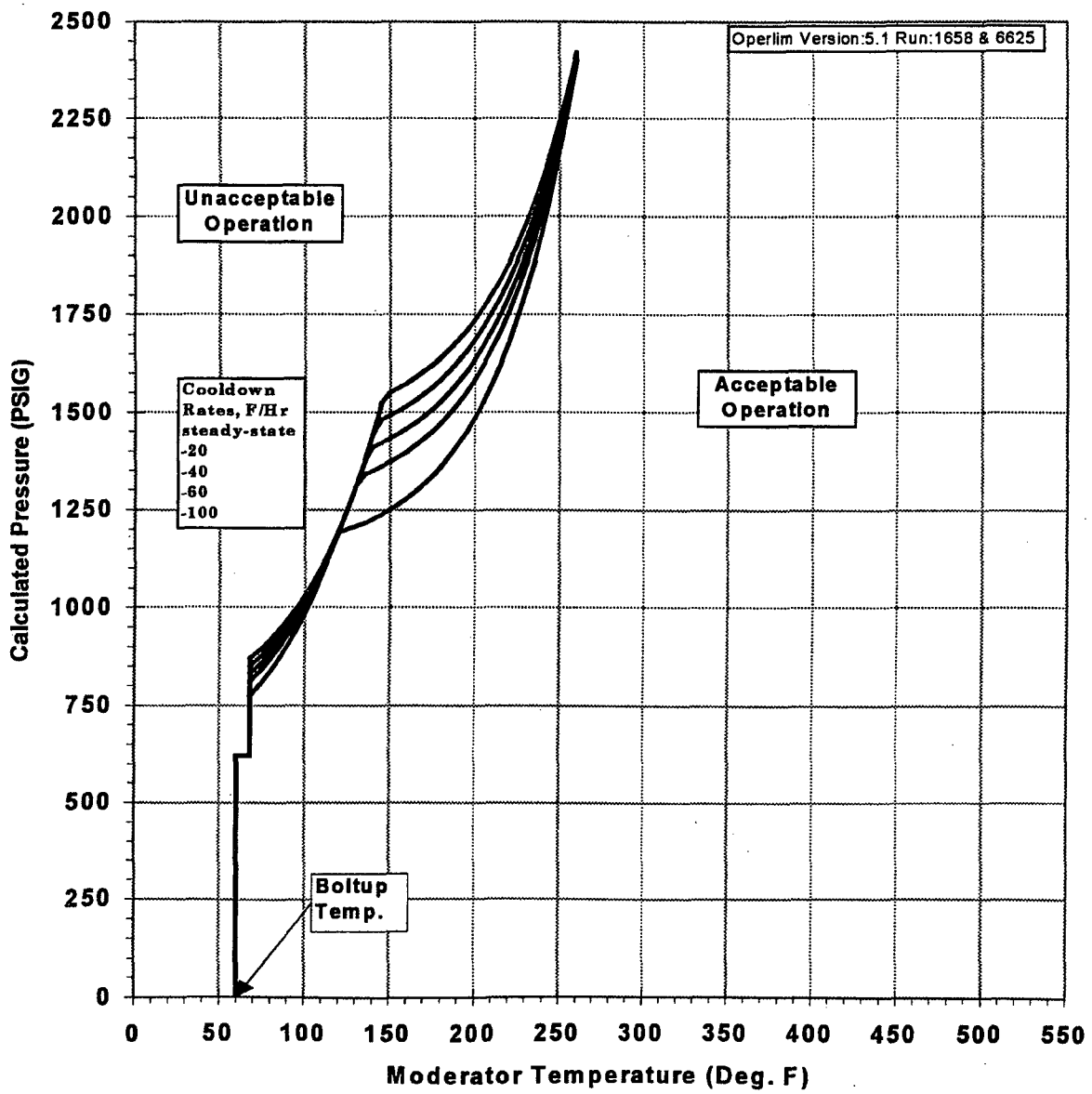

Figure 4 **R.E. Ginna Reactor Coolant System Cooldown Limitations (Cooldown Rates up to 100°F/hr) Applicable for the First 52 EFPY (Without Margins for Instrumentation Errors) Using 1996 App.G Methodology**

TABLE 24
52 EFPY Heatup Curve Data Points Using 1996 App. G & ASME Code Case N-641
(without Uncertainties for Instrumentation Errors)

60 Heatup		60 Critical Limit*		100 Heatup		100 Critical Limit		Leak Test Limit	
T (°F)	P (psig)	T (°F)	P (psig)	T (°F)	P (psig)	T (°F)	P (psig)	T (°F)	P (psig)
60	0	162	0	60	0	162	0	112	1500
60	621	162	621	60	621	162	621	143	2000
65	621	162	621	65	621	162	621	162	2485
68	621	162	861	68	621	162	844		
68	861	162	861	68	844	162	844		
70	861	162	865	70	844	162	844		
75	865	162	875	75	844	162	844		
80	875	162	889	80	844	162	848		
85	889	162	908	85	848	162	856		
90	908	162	930	90	856	162	868		
95	930	162	955	95	868	162	883		
100	955	162	984	100	883	162	902		
105	984	162	1017	105	902	162	924		
110	1017	162	1054	110	924	162	950		
115	1054	162	1095	115	950	162	980		
120	1095	165	1141	120	980	165	1014		
125	1141	170	1192	125	1014	170	1052		
130	1192	175	1248	130	1052	175	1094		
135	1248	180	1310	135	1094	180	1142		
140	1310	185	1378	140	1142	185	1195		
145	1378	**190**	**1445**	145	1195	190	1254		
150	**1445**	**195**	**1460**	150	1254	195	1319		
155	**1460**	**200**	**1476**	155	1319	**200**	**1349**		
160	**1476**	**205**	**1495**	**160**	**1349**	**205**	**1362**		
165	**1495**	**210**	**1515**	**165**	**1362**	**210**	**1377**		
170	**1515**	**215**	**1537**	**170**	**1377**	**215**	**1394**		
175	**1537**	**220**	**1561**	**175**	**1394**	**220**	**1412**		
180	**1561**	**225**	**1589**	**180**	**1412**	**225**	**1433**		
185	**1589**	**230**	**1619**	**185**	**1433**	**230**	**1456**		
190	**1619**	**235**	**1652**	**190**	**1456**	**235**	**1481**		
195	**1652**	**240**	**1689**	**195**	**1481**	**240**	**1510**		
200	**1689**	**245**	**1730**	**200**	**1510**	**245**	**1541**		
205	**1730**	**250**	**1775**	**205**	**1541**	**250**	**1576**		
210	**1775**	**255**	**1824**	**210**	**1576**	**255**	**1614**		
215	**1824**	**260**	**1879**	**215**	**1614**	**260**	**1657**		

*** Data Points in Bold are the limiting pressures and temperature from the Circ. Flaw Run**

TABLE 24 - (Continued)
52 EFPY Heatup Curve Data Points Using 1996 App. G& ASME Code Case N-641
(without Uncertainties for Instrumentation Errors)

60 Heatup		60 Critical Limit*		100 Heatup		100 Critical Limit		Leak Test Limit	
T (°F)	P (psig)	T (°F)	P (psig)	T (°F)	P (psig)	T (°F)	P (psig)	T (°F)	P (psig)
220	1879	265	1929	220	1657	265	1704		
225	1929	270	1980	225	1704	270	1756		
230	1980	275	2036	230	1756	275	1814		
235	2036	280	2099	235	1814	280	1877		
240	2099	285	2168	240	1877	285	1947		
245	2168	290	2244	245	1947	290	2025		
250	2244	295	2328	250	2025	295	2111		
255	2328	300	2421	255	2111	300	2205		
260	2421			260	2205	305	2310		
				265	2310	310	2425		
				270	2425				

*** Data Points in Bold are the limiting pressures and temperature from the Circ. Flaw Run**

TABLE 25
52 EFPY Cooldown Curve Data Points Using 1996 App. G & ASME Code Case N-641
(without Uncertainties for Instrumentation Errors)

Steady State		20°F/hr.		40°F/hr.		60°F/hr.		100°F/hr.	
T (°F)	P (psig)	T (°F)	P (psig)	T (°F)	P (psig)	T (°F)	P (psig)	T (°F)	P (psig)
60	0	60	0	60	0	60	0	60	0
60	621	60	621	60	621	60	621	60	621
65	621	65	621	65	621	65	621	65	621
68	621	68	621	68	621	68	621	68	621
68	870	68	851	68	831	68	812	68	776
70	877	70	858	70	839	70	821	70	785
75	897	75	879	75	861	75	843	75	810
80	918	80	901	80	885	80	869	80	838
85	942	85	926	85	911	85	897	85	869
90	969	90	954	90	941	90	928	90	904
95	998	95	985	95	973	95	962	95	942
100	1030	100	1019	100	1009	100	1000	100	985
105	1066	105	1057	105	1049	105	1042	105	1032
110	1105	110	1098	110	1093	110	1088	110	1084
115	1149	115	1144	115	1141	115	1140	115	1142
120	1197	120	1195	120	1195	120	1197	**120**	**1193**
125	1250	125	1250	125	1250	125	1250	**125**	**1199**
130	1309	130	1309	130	1309	130	1309	**130**	**1207**
135	1374	135	1374	135	1374	**135**	**1341**	**135**	**1216**
140	1446	140	1446	**140**	**1412**	**140**	**1351**	**140**	**1226**
145	1525	**145**	**1482**	**145**	**1422**	**145**	**1361**	**145**	**1237**
150	**1552**	**150**	**1493**	**150**	**1433**	**150**	**1372**	**150**	**1250**
155	**1563**	**155**	**1505**	**155**	**1445**	**155**	**1385**	**155**	**1264**
160	**1576**	**160**	**1518**	**160**	**1459**	**160**	**1399**	**160**	**1279**
165	**1590**	**165**	**1532**	**165**	**1474**	**165**	**1415**	**165**	**1296**
170	**1605**	**170**	**1548**	**170**	**1490**	**170**	**1433**	**170**	**1316**
175	**1622**	**175**	**1566**	**175**	**1509**	**175**	**1452**	**175**	**1337**
180	**1641**	**180**	**1585**	**180**	**1530**	**180**	**1474**	**180**	**1361**
185	**1662**	**185**	**1607**	**185**	**1553**	**185**	**1498**	**185**	**1388**
190	**1685**	**190**	**1631**	**190**	**1578**	**190**	**1524**	**190**	**1418**
195	**1710**	**195**	**1658**	**195**	**1606**	**195**	**1554**	**195**	**1451**
200	**1738**	**200**	**1687**	**200**	**1637**	**200**	**1587**	**200**	**1488**
205	**1769**	**205**	**1720**	**205**	**1671**	**205**	**1623**	**205**	**1528**
210	**1803**	**210**	**1756**	**210**	**1709**	**210**	**1663**	**210**	**1574**
215	**1841**	**215**	**1796**	**215**	**1752**	**215**	**1708**	**215**	**1624**
220	**1883**	**220**	**1840**	**220**	**1798**	**220**	**1757**	**220**	**1679**
225	**1929**	**225**	**1889**	**225**	**1850**	**225**	**1812**	**225**	**1741**
230	**1980**	**230**	**1943**	**230**	**1907**	**230**	**1873**	**230**	**1810**
235	**2036**	**235**	**2003**	**235**	**1970**	**235**	**1940**	**235**	**1886**
240	**2099**	**240**	**2069**	**240**	**2040**	**240**	**2014**	**240**	**1970**
245	**2168**	**245**	**2142**	**245**	**2118**	**245**	**2097**	**245**	**2063**
250	**2244**	**250**	**2222**	**250**	**2204**	**250**	**2188**	**250**	**2166**
255	**2328**	**255**	**2312**	**255**	**2298**	**255**	**2289**	**255**	**2281**
260	**2421**	**260**	**2410**	**260**	**2403**	**260**	**2400**	**260**	**2400**

* **Data Points in Bold are the limiting pressures and temperature from the Circ. Flaw Run**

7 REFERENCES

1. Regulatory Guide 1.99, Revision 2, "Radiation Embrittlement of Reactor Vessel Materials," U.S. Nuclear Regulatory Commission, May 1988.

2. WCAP-14040-NP-A, Revision 2, "Methodology used to Develop Cold Overpressure Mitigating system Setpoints and RCS Heatup and Cooldown Limit Curves", J.D. Andrachek, et. al., January 1996.

3. ASME Code Case N-641, "Alternative Pressure-Temperature Relationship and Low Temperature Overpressure Protection System Requirements Section XI, Division 1", January 17, 2000.
[*Sub Reference 1: ASME Code Case N-640, "Alternative Reference Fracture Toughness for Development of P-T Limit Curves for Section XI, Division 1", February 26, 1999.*]
[*Sub Reference 2: ASME Boiler and Pressure Vessel Code, Case N-588, "Attenuation to Reference Flaw Orientation of Appendix G for Circumferential Welds in Reactor Vessels", Section XI, Division 1, Approved December 12, 1997.*]

4. Section XI of the ASME Boiler and Pressure Vessel Code, Appendix G, "Fracture Toughness Criteria for Protection Against Failure." Dated December 1995, through 1996 Addendum.

5. Code of Federal Regulations, 10 CFR Part 50, Appendix G, "Fracture Toughness Requirements," U.S. Nuclear Regulatory Commission, Washington, D.C., Federal Register, Volume 60, No. 243, dated December 19, 1995.

6. "Fracture Toughness Requirements", Branch Technical Position MTEB 5-2, Chapter 5.3.2 in Standard Review Plan for the Review of Safety Analysis Reports for Nuclear Power Plants, LWR Edition, NUREG-0800, 1981.

7. WCAP-15092, Revision 3, "Turkey Point Units 3 and 4 WOG Reactor Vessel 60-Year Evaluation Minigroup Heatup and Cooldown Limit Curves for Normal Operation", T.J. Laubham, et. al., May 2000.

8. WCAP-7254, "Rochester Gas and Electric Robert E. Ginna Unit No. 1 Reactor Vessel Radiation Surveillance Program", S.E. Yanichko, May 1969.

9. WCAP-14684, "R.E. Ginna Heatup and Cooldown Limit Curves for Normal Operation", Ed Terek, et. al., June 1996.

10. WCAP-10496, "R.E. Ginna Reactor Vessel Surveillance Capsule T Reconstituted Weld Metal Charpy Impact Tests", S.E. Yanichko, et. al, March 1984.

11. Regulatory Guide 1.190, "Calculational and Dosimetry Methods for Determining Pressure Vessel Neutron Fluence," March 2001.

12. WCAP-14044, "Westinghouse Surveillance Capsule Neutron Fluence Reevaluation",E.P. Lippincott, April 1994.

13. RSICC Computer Code Collection CCC-650, "DOORS 3.1, One, Two- and Three-Dimensional Discrete Ordinates Neutron/Photon Transport Code System," August 1996.

14. RSIC Data Library Collection DLC-185, "BUGLE-96, Coupled 47 Neutron, 20 Gamma-Ray Group Cross-Section Library Derived from ENDF/B-VI for LWR Shielding and Pressure Vessel Dosimetry Applications," March 1996.

15. A. Schmittroth, "FERRET Data Analysis Code," HEDL-TME-79-40, Hanford Engineering Development Laboratory, Richland, WA, September 1979.

16. RSIC Data Library Collection DLC-178, "SNLRML Recommended Dosimetry Cross-Section Compendium," July 1994.

17. 1989 Section III, Division 1 of the ASME Boiler and Pressure Vessel Code, Paragraph NB-2331, "Material for Vessels."